Journal Pre-proofs

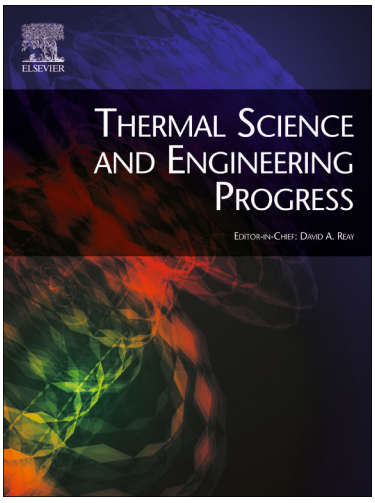

An experimental investigation on bubbles departure characteristics during sub-cooled flow boiling in a vertical U-shaped channel utilizing high-speed photography

Shahriyar Ghazanfari Holagh, Mohammad Ali Abdous, Prosun Roy, Masood Shamsaiee, Mahmood Shafiee, Hamid Saffari, Luis Valiño, Ronnie Andersson

PII: S2451-9049(20)30348-6
DOI: https://doi.org/10.1016/j.tsep.2020.100828
Reference: TSEP 100828

To appear in: *Thermal Science and Engineering Progress*

Received Date: 12 May 2020
Revised Date: 2 November 2020
Accepted Date: 20 December 2020

Please cite this article as: S. Ghazanfari Holagh, M. Ali Abdous, P. Roy, M. Shamsaiee, M. Shafiee, H. Saffari, L. Valiño, R. Andersson, An experimental investigation on bubbles departure characteristics during sub-cooled flow boiling in a vertical U-shaped channel utilizing high-speed photography, *Thermal Science and Engineering Progress* (2020), doi: https://doi.org/10.1016/j.tsep.2020.100828

This is a PDF file of an article that has undergone enhancements after acceptance, such as the addition of a cover page and metadata, and formatting for readability, but it is not yet the definitive version of record. This version will undergo additional copyediting, typesetting and review before it is published in its final form, but we are providing this version to give early visibility of the article. Please note that, during the production process, errors may be discovered which could affect the content, and all legal disclaimers that apply to the journal pertain.

© 2020 Elsevier Ltd. All rights reserved.

An experimental investigation on bubbles departure characteristics during sub-cooled flow boiling in a vertical U-shaped channel utilizing high-speed photography

Shahriyar Ghazanfari Holagh[a, *1], Mohammad Ali Abdous[a], Prosun Roy[b], Masood Shamsaiee[a], Mahmood Shafiee[c], Hamid Saffari[a], Luis Valiño[d], Ronnie Andersson[e]

[a] School of Mechanical Engineering, Iran University of Science and Technology, Tehran, Iran

[b] Department of Mechanical Engineering, University of Wisconsin, Milwaukee, WI, USA

[c] School of Engineering Science and Digital Arts, University of Kent, Canterbury CT2 7NT, UK

[d] Laboratorio de Investigación en Fluidodinámica y Tecnologías de la Combustión (LIFTEC), Zaragoza, Spain

[e] Department of Chemistry and Chemical Engineering, Chalmers University of Technology, Gothenburg, Sweden.

Abstract:

Classified as a passive heat transfer enhancement technique, U-shaped channels are commonly encountered with applications associated with boiling heat transfer such as air conditioning systems, evaporators, and boilers. On the other hand, the understanding of heat transfer in flow boiling is heavily dependent upon bubbles dynamic behavior, which is influenced by flow and geometrical conditions. In this paper, bubbles departure characteristics are experimentally studied in the upward sub-cooled flow boiling of distilled water in a vertical U-shaped channel. The influence of flow conditions, embracing heat flux, mass flux, and inlet sub-cooling on bubbles these characteristics, encompassing departure diameter, growth and waiting times, and nucleation frequency, is investigated through conducting 68 experiments. All the experiments are carried out at atmospheric pressure over a Nichrome heating surface installed on the outer wall of the channel, with heat flux, mass flux, and inlet flow temperature in the ranges of 26.1-61.5 $kW.m^{-2}$, 114-255 $kg.m^{-2}s^{-1}$, and 1 to 8 ℃. A high-speed camera is utilized to capture bubbles growth process and departure instance. The results reveal that as wall heat flux increases and mass flux and inlet sub-cooling decreases, the bubbles departure diameter and frequencies rise, while waiting times decline. Also, lower growth times are detected when wall heat flux and mass flux increase and inlet sub-cooling declines. Two new correlations are developed to predict present and previously published experimental data of departure diameter and nucleation frequencies with mean standard deviations of 18.0% and 18.5%, correspondingly.

[*1] Corresponding author:

E–mail: Ghazanfari_shahriyar@alumni.iust.ac.ir Tel: +989013571088

Journal Pre-proofs

Keywords: Sub-cooled flow boiling; U-shaped channel; Departure diameter; Nucleation frequency; Growth time; Waiting time

1. Introduction

Due to the high heat transfer rate of boiling phenomenon, and similarly due to its complex nature, the study of flow boiling has been an interesting yet challenging field over the past five decades [1], particularly in enhanced heat exchangers [2]. Boiling phenomenon initiates when first bubbles form, and previous studies [3,4] reveal that the mechanisms of nucleation, growth, and departure of bubbles play a key role in boiling heat transfer and void fraction distribution. Thus, identifying bubbles departure phenomenon, characterized by departure diameter (the bubble diameter when leaving the nucleation site), growth time (the time elapsed between the formation and the departure moments), waiting time (the time elapsed between the formation of a bubble and departure of the previous one), and nucleation frequency (the number of bubbles departed from a nucleation site in one second), contributes to a better understanding of boiling heat transfer in subcooled flow boiling [1,5,6]. Moreover, the accuracy of different numerical models developed to simulate boiling phenomenon highly depends on the mentioned characteristics [3,7]. As a salient example, in one of the useful models, Wall Heat Flux Partitioning model, the wall heat flux is divided into three parts, namely single-phase, quenching, and evaporating heat flux [8]. The sub-models used to estimate the evaporating and quenching heat flux require appropriate relations for two parameters, i.e. departure diameter and nucleation frequency [7]. Furthermore, bubble departure diameter and nucleation frequency have an important role in determination of the Interfacial Area Concentration (IAC) which is used in two-fluid model to predict interfacial area transfer terms [9]. Hence, suitable selection of these terms reduces the error of numerical solutions [3].

On the other hand, it has been substantiated that bubbles departure characteristics are strongly dependent upon heat transfer mechanisms and interactions between the bubbles and their surrounding liquid layers [10,11]. A bubble and its surrounding liquid layers during sub-cooled flow boiling are schematically shown in Fig. 1. As can be seen, three liquid layers surround a bubble. The first, named evaporative micro-layer, is a thin wedge-shaped liquid micro-layer that is trapped between the heating surface and the lower parts of the bubble which starts to evaporate when nucleation is initiated, leading to an enhancement in wall temperature fluctuation [11–14]. As the bubble grows, the temperature of the liquid region near the heating surface slightly depletes.

Journal Pre-proofs

This region is the second layer that is called superheated layer [12,13]. Subcooled region, for which the bulk liquid temperature is lower than saturation temperature, is the third liquid layer surrounding the top of the bubble. In essence, the bubble receives heat and vapor from the evaporative and superheated layers, contributing to an enhancement in the bubble diameter, while condensation occurs in the sub-cooled region, leading to a reduction in the bubble diameter [12,15]. As well as these, interactions between the vapor and liquid phases and forces imposed on the bubbles influence bubbles departure phenomenon [3,16]. Thus, any factor influencing mentioned heat transfer mechanisms and interactions like flow conditions, local turbulence around the bubble, temperature gradient between the bubble and liquid layers, and geometrical configurations is bound to significantly affect bubbles departure characteristics. Meanwhile, in U-shaped channels, flow experiences some phenomena such as radial pressure gradient and resulting secondary flow and Dean Vortices that considerably influence bubbles departure characteristics [17,18]. Therefore, regarding the strong dependency of bubbles departure characteristics on flow behavior and their impact on flow boiling heat transfer, void fraction distribution, and the accuracy of numerical models simulating boiling phenomenon, the importance of studying these characteristics and proposing appropriate correlations to predict bubbles departure diameter and nucleation frequency in U-shaped channels becomes evident and vital.

Numerous investigations have been performed to identify the relation between bubbles departure diameter and flow conditions in straight channels. Ghunther [19] studied bubbles departure diameter in sub-cooled flow boiling of water at high ranges of flow conditions in a straight channel and found that bubbles diameter increases as wall heat flux rises and mass flux declines. Tolubinsky and Kostanchuk [20] proposed correlations for departure diameter and frequency of water flow boiling on a horizontal steel plate under different working pressures. The effects of mass flux and heat flux on the growth and collapse of bubbles in sub-cooled flow boiling of water were investigated by Abdelmessih et al. [21] using high-speed photography. They found that an increase in mass flux results in smaller bubble diameters with lower lifetime, and an increase in wall heat flux leads to bigger bubbles with higher lifetime. Unal [5] assumed a spherical bubble growing in a small micro-layer between a bubble and a heating wall. Based on his assumptions, three semi-empirical correlations were developed using previous studies experimental data to predict bubbles growth rate, departure diameter, and maximum bubble growth time in subcooled flow boiling of water at high pressures. Klausner et al. [22] carried out an

experimental study on bubbles departure diameter in saturated flow boiling of R-113. The results showed that the departure diameter increases as wall heat flux rises, and mass flux and inlet sub-cooling decline. They also proposed a model to predict bubbles departure diameter. An investigation on bubbles nucleation, departure, and lift-off in subcooled boiling of FC-87 in a vertical rectangular channel was carried out by Thorncroft et al. [23]. The results indicated that increasing heat flux and decreasing mass flux culminate in higher departure diameters for both upward and downward flow configurations. Prodanovic et al. [24] studied the growth, departure, and lift-off of bubbles in subcooled flow boiling of water in an annular upward channel under different pressures using high-speed photography. They developed some correlations to predict bubble departure diameter and time based on Jakob and Boiling numbers. The relation proposed by Unal was modified by Morel et al. [25] for saturation conditions. Basu et al. [26] assumed that the incoming energy from the heating wall first enters a thin layer of superheated fluid on the wall and then a fraction of it takes part in vapor formation and growth and consequently, the rest of the total heat flux heats up the fluid bulk via convection mechanism. Based on this assumption, they proposed a relation to predict the bubble departure diameter in sub-cooled flow boiling. Bubbles departure diameter in sub-cooled flow boiling of water at low heat and mass fluxes was experimentally studied by Cho et al. [1]. They proposed a model for predicting departure diameter at low flow conditions range. Zou and Jones [27] performed an experimental study to investigate the effect of heating surface material on bubble departure and nucleation frequency in sub-cooled flow boiling of R-134a using copper and stainless steel surfaces. The findings demonstrated that the departure diameter and nucleation frequency are insignificantly dependent on the surface material. A series of experimental studies on bubbles departure diameter during sub-cooled flow boiling in vertical and inclined channels were conducted by Sugrue et al. [3,4]. They found that the biggest bubbles depart in the downward-facing horizontal heater configuration and the smallest bubbles from a vertically positioned heater. Guan et al. [28] investigated bubbles departure diameter in water sub-cooled flow boiling at atmospheric pressure and proposed a model for departure diameter prediction. An experimental study of wall nucleation characteristics, embracing departure diameter and frequency, during subcooled flow boiling of water in a vertical straight channel was carried out by Brooks et al. [29] at various working pressures. It was found that the effect of wall heat flux and liquid sub-cooling on bubbles departure diameter is stronger at low pressures compared to elevated ones. Goel et al. [30] performed an experimental study on bubbles

departure characteristics in forced upward convective sub-cooled flow boiling in a vertical channel at low flow velocities. They reported that increasing wall heat flux and consequently, wall superheat leads to higher evaporation and thus, larger bubble departure diameters. In addition, their results showed that increasing mass flux results in higher drag force which reduces bubbles departure diameter. Bubbles departure diameter and nucleation frequency were compared among various nucleation sites under the same flow conditions for water sub-cooled flow boiling in a vertical straight channel by Ooi et al. [31]. The findings showed that these parameters vary significantly from one site to another at the same flow conditions, emphasizing the need to consider many nucleation sites to obtain mean values for departure diameter and nucleation frequency. Colgan et al. [32] performed an experimental study on bubbles departure diameter and nucleation frequency during water sub-cooled flow boiling in a vertical straight channel at sub-atmospheric pressure. They observed that by decreasing sysem pressure, departure diameter rises while nucleation frequency declines. Zhou et al [33] carried out a series of experiments to study bubbles departure diameter during subcooled flow boiling in a horizontal straight channel under both low and high flow conditions, and developed an imprical model using Buckingham theorem to predict departure diameter. Their findings indicated that bubbles departure diameter declines as the system pressure, flow velocity, and inlet sub-cooling increase and wall superheat decreases. Ren et al [34] experimentally studied the influence of flow conditions on bubbles departure characteristics during sub-cooled flow boiling in a narrow channel. They found that greater wall superheat results in larger bubble growth rate and an increase in mass flow rate leads to faster bubble departure. They also proposed a correlation to predict bubbles departure diameter.

Bubble growth and waiting times and nucleation frequency have also been studied in pool boiling [35–38] and flow boiling in straight channels [5,26] by various researchers. Zeng et al. [39] studied bubble growth time for horizontal flow boiling of R113. They developed a relation to estimate the bubble growth time based on Jakob number and bubble growth constant. Bubbles nucleation frequency in upward sub-cooled flow boiling of water in an annular straight channel was examined by Situ et al. [40]. They realized that the correlations developed for pool boiling are of low accuracy for flow boiling. They correlated dimensionless bubble nucleation frequency with dimensionless nucleate boiling heat flux. Chu et al. [9] investigated bubbles nucleation frequency in sub-cooled flow boiling of water in a vertical straight channel and proposed a correlation based on Jakob number, boiling number, density ratio, and dimensionless sub-cooling degree. Euh et al.

Journal Pre-proofs

[41] examined the effect of wall heat flux, mass flux, inlet sub-cooling, and system pressure on bubbles nucleation frequency during upward sub-cooled water flow boiling in an annular straight channel. Their results showed an increase in bubble nucleation frequency for higher wall heat flux and system pressure as well as lower flow velocity and inlet sub-cooling. Moreover, they proposed dimensionless nucleation frequency model based on the model previously proposed by situ et al. [40]. The findings of Brooks et al. [29] on bubbles growth time in subcooled flow boiling revealed that bubbles growth time declines as the liquid bulk temperature surrounding the bubbles rises, and the nucleation frequency is a strong function of liquid sub-cooling and wall heat flux. The results obtained by Goel et al. [30] on bubbles waiting time in sub-cooled flow boiling showed that compared to growth time, waiting time is the dominant factor in predicting the nucleation frequency. They concluded that by increasing wall superheat, bubbles tend to have shorter waiting times and hence, the nucleation frequency increases. The same effect has been reported for lower mass flux and inlet sub-cooling.

As for curved channels, there exists a few studies investigating bubbles characteristics. Abdous et al. [17] studied bubbles departure and lift-off radii in sub-cooled flow boiling of distilled water in a vertical U-shaped channel. The findings demonstrated that similar to straight channels, in the U-shaped channel, bubbles departure and lift-off radii rise as wall heat flux increases and mass flux and inlet sub-cooling decrease. A comparative study on the effect of radial pressure gradient on bubbles dynamic behavior was carried out by Holagh et al [18]. They compared bubbles characteristics between a vertical U-shaped channel and a straight channel under the same flow conditions. The results substantiated that the radial pressure gradient present in the U-shaped channel contributes to bigger bubble departure diameter, higher nucleation frequencies, and lower growth and waiting times compared with the straight channels. However, neither Abdous et al. [17] nor Holagh et al [18] discussed the influence of variation in flow conditions on bubbles growth time, waiting time, and nucleation frequency in U-shaped channels. In addition, accurate correlations for predicting bubbles departure diameter and nucleation frequency in U-shaped channels were not proposed by these studies. Detailed information on all the reviewed studies is provided in Tables 1a and 1b.

As the literature review shows, previous experimental investigations on bubbles dynamic behavior are largely devoted to straight channels, and only few studies have investigated bubbles

characteristics in a U-shaped channel. Also, the influence of flow conditions on bubbles growth and waiting time as well as nucleation frequency in a U-shaped channel has not been studied yet. In addition to these, there exists no correlation in the literature accurately predicting bubbles departure diameter and nucleation frequency in U-shaped channels. On the other hand, as previously discussed, such deficiencies are bound to cause unreliable and inaccurate numerical simulations of flow boiling in U-shaped channels. To remedy these deficiencies, in the current paper, bubbles departure characteristics during sub-cooled flow boiling of distilled water in a vertical U-shaped channel are investigated using high-speed photography. The effects of variations in flow conditions, embracing wall heat flux, mass flux, and inlet sub-cooling on bubbles departure diameter, growth and waiting times, and nucleation frequency are experimentally studied. The accuracy and applicability of the proposed correlations developed for pool boiling and flow boiling in straight channels are also investigated for the U-shaped channel through predicting the present experimental data by existing correlations and models in the literature. Significant errors between the present experimental data and those predicted by the correlations necessitated developing new empirical correlations. Hence, two new correlations for bubbles departure diameter and nucleation frequency are developed to accurately predict the present experimental data. Ultimately, it is worth noting that this study considers a low range of wall heat flux to deter the negative effects of bubbles coalescence and interactions, occurring at high heat fluxes, on image processing and data acquisition, and also to have a better understanding of flow conditions effects on departure characteristics since such effects are stronger at low ranges of flow conditions [3,16,21,29].

2. Experimental description

Current section deals with describing applied experimental facilities, test section and conditions, nucleation site locations, data acquisition, and techniques employed in image processing.

2.1. Experimental setup

In order to study the bubbles departure phenomenon, a suitable test rig has been designed and constructed regarding the desired test conditions. Fig. 2 depicts the process diagram of the setup. Prior to conducting the experiments, the tank and all loops and pipes are filled with distilled water. The centrifugal pump then starts and sucks the water from the tank and delivers it to the pre-heater. Depending on the desired inlet temperature, the pre-heater increases the temperature of the flow using an electrical heater with a maximum capacity of 3 kW coupled to a temperature controller.

Then, flow enters a deaerator, collecting all the potential vapor bubbles and feeding the test section with pure hot liquid water. Before flow enters the test section, it passes through a turbine flow meter which is connected to a computer. The flow then enters the test section, where actual boiling occurs. The demand for heat in the test section is provided by a 1 kW DC power supply. The outlet flow of the test section enters a condenser which employs a separate coolant loop to lower the flow temperature. The flow finally reenters the tank. Various electronics and instrumentation have been employed to help reaching the desired conditions, to control the experiments, and to acquire data. The equipment and their respective accuracies are presented in Table 2, and the uncertainty analysis for important parameters is also presented in Table 2. In order to capture bubbles formation, growth, and departure instances, a digital high-speed camera (PCO 1200 HS) has been utilized. It is set to take pictures at the rate of 20000 frames per second. The lighting has been provided by a set of LEDs to ensure the suitability of the photos for later analysis and data acquisition.

2.2. Test section

Fig. 3 shows the U-shaped channel and its components in a demounted view. Test section walls, made of poly methyl methacrylate, also known as Plexiglas, are mounted using bolts and nuts, creating a rectangular cross section with constant dimensions of 14×18 mm and hydraulic diameter of 15.75 mm. The middle part of the U-shaped channel is designed as a semicircle with outer radius of 300 mm. Two straight parts of the channel, located before and after the semicircle part, are 350 mm long. A smooth 13×1042 mm Nichrome strip has been placed on the outer wall of the channel (in semicircle part). It acts as the heating surface on which the boiling phenomenon occurs. The Nichrome strip is heated using the DC power supply mentioned earlier. In order to prevent heat loss and to make sure that all the supplied power is delivered to the flow, a 15-mm-thick thermal insulation has been placed behind the heating surface. In addition, rubber gaskets have been employed for sealing purposes.

2.3. Nucleation sites

Bubbles are studied on two locations placed relatively apart from each other to ensure the precision of the observed effects of flow conditions on bubble dynamic behavior along the heating surface. These locations, as illustrated in Fig. 4a, denoted as S1 and S2, are placed in peripheral angles of 150°-155° and 125°-130°, respectively, each covering 5 peripheral degree. For the sake of the

comprehensiveness of the tests and in order to take the influence of nucleation site locations as well as wall orientation on departure characteristics into consideration, these locations were chosen 25° apart. Some of the tests have been performed on S1, while others have been done on S2. It is to be noted that in each location, the bubbles generated in several adjacent nucleation sites were captured for each test.

2.4. Thermocouples locations and installation

In order to measure the bulk temperature of the flow in the entrance, outlet, and in the vicinity of the nucleation sites, as well as the wall temperature, ten K-type thermocouples have been installed in locations shown in Fig. 4a. As demonstrated in this figure, these thermocouples are designated as follows: one for inlet flow temperature (T_{in}), two for bulk flow temperature in the vicinity of the nucleation sites S1 and S2 ($T_{f-S1}$and T_{f-S2}), one for outlet flow temperature (T_{out}) and four for wall temperature in S1 (T_{W5} and T_{W6}) and S2 (T_{W3} and T_{W4}) locations. Furthermore, in order to measure wall temperature before the locations S1 and S2, two thermocouples (T_{W1} and T_{W2}) are located in peripheral angles of 45° and 90°. The installation of the thermocouples measuring heating surface temperature (Nichrome strip) is demonstrated in Fig. 4b. As can be observed, these thermocouples pass through the outer wall and then the 15-mm thermal insulator and place behind the heating surface.

2.5. Heating surface treatment and characteristics

The Nichrome heating surface, where bubbles generate, was treated by progressively finer sandpapers, from 100 to 2000 grit, followed by a degreasing process in an acetone bath. Consequently, a surface with a mirror finish that was later inspected using Atomic Force Microscopy (AFM) together with Scanning Electron Microscopy (SEM) as demonstrated in Figs. 5a and 5b was achieved. Fig. 5c exhibits surface sample profiles. The analysis conducted on the data on the surface profile sampled from three different locations on the heating surface revealed the values of 0.017 μm and 0.01 μm for average roughness (R_a) and root mean squared roughness (R_q) computed by Eqs. (1)-(2), respectively, where z_i depicts the height of the i^{th} element of total n elements of the surface profile.

Journal Pre-proofs

$$R_a = \frac{1}{n}\sum_{i=1}^{n}|z_i| \quad (1)$$

$$R_q = \sqrt{\frac{1}{n}\sum_{i=1}^{n}z_i^2} \quad (2)$$

As illustrated in Fig. 5d, the contact angle between a water droplet and the treated heating surface was measured to be equal to 52.6°.

2.6. Experimental procedure and test matrix

The general test conditions are presented in Table 3. In order to study the effect of flow conditions on the bubble departure phenomenon in S1 and S2 locations, 68 experimental tests were carried out in accordance with Tables 4a, 4b and 4c. 20 experimental tests were conducted with HFE1-S1, HFE2-S1, HFE3-S2 and HFE4-S2 test groups to investigate the effect of heat flux for constant inlet temperature and mass flux. The first two groups of these experiments are conducted in S1 and the two others are carried out in S2 with the conditions listed in Table 4a. For the case of mass flux effect, 20 experiments are conducted with FVE1-S1, FVE2-S1, FVE3-S2 and FVE4-S2 test groups for constant wall heat flux and fixed inlet temperature to only take the effect of mass flux variation into account with the conditions listed in Table 4b in both S1 and S2 locations. In order to investigate the effect of the inlet temperature, 28 experiments were performed in both S1 and S2 the conditions of which the conditions are given in Table 4c. Wall heat flux and mass flux are constant in these test groups.

In each test, the high-speed camera is utilized to precisely capture the behavior of the bubbles in formation, growth, and departure phases. To minimize errors in the experimental data, the tests were repeated three times for each test condition in three different days, in each of which 4 bubbles from different adjacent nucleation sites were captured and considered for analysis. Thus, for each test condition, bubble growth and departure are photographed twelve times and these sets of photos are extracted for each flow conditions. Eventually, departure diameter, growth and waiting times, and nucleation frequencies were acquired by averaging the values obtained for twelve bubbles for each test.

It should be noted that the flow conditions and geometrical conditions were devised so that for all test conditions the flow is always turbulent and sub-cooled in the channel. Additionally, as the

Journal Pre-proofs

impact of flow conditions on bubbles characteristics is severer and more observable at low flow conditions [3,16,21,29], the test conditions were considered in relatively low ranges so as to have a better comprehension of variations in bubbles dynamic behavior characteristics.

2.7. Image processing

As demonstrated in Fig. 6, the high-speed camera focuses on nucleation sites locations, S1 and S2, to capture bubbles formation, growth, and departure. It is tilted 13° with regard to the horizon to have a complete view over the heating surface and the whole height of the channel. The camera is located 12 cm away from the front wall. As for acquiring the bubbles departure diameter from graphical data, the inner face of the back wall is engraved in 1-millimeter units and acts as a length scale (see Fig. 7).

Digital image analysis was carried out via developing a code in MATLAB software to attain all the necessary information. The processing method is elucidated as follows. First, utilizing a series of MATLAB predefined functions, the obtained photos are enhanced so that the bubbles edges are distinguished better. Such enhancements merely influence the brightness, color, and texture of the images without distorting them in any way. Figs. 8a and 8b respectively demonstrate a generic image and its enhanced version, captured in one of the experiments. As can be obviously seen, the second version has enhanced in contrast since the bubbles edges are observed more clearly. Afterwards, the bubbles edges are identified. Highlighting the object (the bubble) via finding the image background so as to subtract it from the image processing analysis is a helpful step here. The detected background along with the result of the developed bubble detection code are correspondingly exhibited in Figs. 8c and 8d. The code is capable of detecting all the shapes resembling a circle in the image and giving their center location and diameter. The code is also able to identify circles having diameters within a certain predefined range, making the detection more accurate. Since the code gives the values of diameters in pixel, the next step is to determine the ratio of pixel to mm pixel, which is accomplished through finding the number of pixels corresponding to the engraved length scale. To provide a more accurate calculation, as shown in Figs. 8e and 8f, the distance between three 1-mm marks were attained in pixels. The average value is found to be 0.0182 mm for each pixel. By multiplying the acquired diameters in pixels by 0.0182, the actual diameters of the bubbles are obtained. Additionally, the data for bubble growth and waiting times are obtained using the series of successive photos of the captured bubble after

the determination of bubbles formation and departure moments by multiplying the number of images between the corresponding images by the time interval between two successive images, which is equal to 0.05 ms. It is worth mentioning that in order to detect the departure instance, the code tracks the base of the bubble through the successive images after the bubble's formation moment.

Fig. 9 depicts a bubble captured in test denoted as HFE1-S1-4 in site S1. Starting from first photo at $t = 0$ ms, a bubble forming on the nucleation site S1 is shown. As shown in the next photos, the bubble then starts to grow and after a certain amount of time known as the growth time, it departs from the nucleation site and then slips on the wall and eventually lifts the wall off. The error of identifying the growth and waiting times is the interval between two consecutive frames (0.05 ms) and the error of determining the diameter is two pixels equal to 0.0364 mm.

3. Results and discussion

In the current section, first, the behavior of bubbles departure diameter, growth and waiting times, and nucleation frequency versus flow conditions is investigated and plotted in Figs. 10-12. Next to that, the proposed correlations for predicting bubbles departure diameter and nucleation frequency in the literature for pool boiling and flow boiling in straight channels are used to predict the present experimental data obtained from the U-shaped channel. Finally, two new correlations are developed to predict obtained data for bubbles departure diameter and nucleation frequency in the U-shaped channel.

3.1. Effect of wall heat flux

The effect of an increase in wall heat flux on bubbles departure diameter, growth and waiting times, and nucleation frequency are plotted in Figs. 10a, 10b, 10c, and 10d, respectively, using data obtained from tests with conditions provided in Table 4a.

Fig. 10a shows a comparison of departure diameter versus wall heat flux for different tests with fixed mass flux and inlet temperature in each case. According to this figure, for constant mass flux and inlet temperature, an increase in heat flux brings about an enhancement in departure diameter. In fact, by increasing wall heat flux, the wall superheat and local liquid temperature increase, resulting in more evaporation in the evaporative micro-layer surrounding the bubble on the heating

surface. This, in turn, leads to an increase in the vapor phase entering the bubble and consequently, the departure diameter increases, similar to what has been observed in straight channels [9,42].

As Fig. 10b illustrates, bubbles growth time declines with increasing wall heat flux. This is because sufficient amount of energy is acquired by liquid flow on the heating wall at higher values of heat fluxes, allowing the liquid fluid to overcome the intermolecular force of the molecules, causing faster local liquid phase change, i.e. higher evaporation rate, that leads to a reduction in bubbles growth time [17,43].

As demonstrated in Figs. 10a and 10b, all the cases show similar trends when wall heat flux varies. However, the case named "HFE1-S1" has larger values of departure diameter and growth time compared to the other cases. This is because compared with the other cases, this case has the lowest amounts of inlet flow temperature and mass flux. This means that the bubbles of this case are subjected to weaker drag forces that aim to detach the bubbles from the nucleation sites, and stronger surface tension forces that contribute to maintaining the bubbles in the nucleation sites [17]. Hence, these bubbles remain in the nucleation sites for larger times which means slower departure, i.e. larger growth time, in comparison with other cases as demonstrated in Fig. 10b. On the other hand, the larger the growth time is, the higher the amount of vapor phase entering the bubble is, resulting in larger departure diameters as indicated in Fig. 10a.

Regarding Fig. 10c, it is evident that bubbles waiting time reduces as wall heat flux increases. Higher heat flux implies higher wall superheat and local liquid temperature, leading to a higher convective heat transfer rate and a faster recuperation of the superheated boundary layer, and thereby contributing to a considerable reduction in waiting period [26,29,30].

The nucleation frequency of bubbles can be calculated by growth and waiting times based on Eq. (3) [40],

$$f_d = \frac{1}{t_W + t_g} \tag{3}$$

where, t_W represents the waiting time and t_d indicates the growth time (departure time) of the bubbles. The review of the recorded images and obtained data shows that in the present experiments, the waiting time is one order of magnitude greater than the growth time of the bubbles, which means that the waiting time has stronger effect on bubbles nucleation frequency.

Also, Geol et al. [30] conducted an study on bubbles waiting time and confirmed that the main factor in the determination of nucleation frequency is the waiting time.

According to Eq. (3), bubbles nucleation frequency has an inverse relationship with sum of growth and waiting times. Since both bubbles growth and waiting times decrease by increasing wall heat flux, bubbles nucleation frequency increases as wall heat flux augments (See Fig. 10d).

3.2. Effect of mass flux

The behaviors of bubbles departure diameter, growth and waiting times, and nucleation frequency against variation in mass flux are correspondingly shown in Figs. 11a, 11b, 11c, and 11d. The test conditions behind these figures are listed in Table 4b.

Figs. 11a and 11b reveal the influence of mass flux on departure diameter and growth time, respectively. From these figures, one can conclude that higher mass fluxes lead to smaller departure diameter and lower growth time. This can be attributable to the effect of higher quasi-steady drag force imposed on bubbles at higher mass fluxes, resulting in faster departure, i.e. lower growth time, with smaller diameter [3,17,29].

As depicted in Fig. 11c, bubbles waiting time increases as the mass flux rises. This is due to the fact that an increase in mass flux leads to a reduction in the wall superheat, and consequently an increase in waiting time since there is an inverse relationship between bubbles waiting time and wall superheat [26,30].

As mentioned earlier, considering the present experiments, the waiting time and its variation are higher in magnitude compared to the growth time. Regarding the major role of waiting time in the determination of nucleation frequency and its reduction for higher mass fluxes, it can be apparently inferred that, bubbles nucleation frequency decreases by increasing mass flux as demonstrated in Fig. 11d.

3.3. Effect of inlet sub-cooling

The relationships between bubbles departure diameter, growth and waiting times, and nucleation frequency with inlet flow temperature are correspondingly exhibited in Figs. 12a, 12b, 12c, and 12d, based on the test conditions provided in Table 4c.

Journal Pre-proofs

Fig. 12a and 12b reveal the influence of inlet flow temperature on bubbles departure diameter and growth time, respectively. As can be seen, with increasing inlet flow temperature, bubbles tend to depart from nucleation sites with bigger diameters (Fig. 12a) in shorter times (Fig. 12b). The reason is the higher local liquid bulk temperature on the heating wall which becomes closer to the saturation temperature as the inlet flow temperature increases. Higher evaporation rate due to the higher bulk temperature, which is equivalent to lower inlet sub-cooling, helps bubbles depart with bigger diameters [3,29,30]. Furthermore, the condensation rate from the top of the bubbles to the sub-cooled layer of the flow is lower for cases with higher bulk temperature, resulting in bigger departure diameters [17]. Also, faster growth owing to this higher evaporation rate reduces bubbles growth time versus an increase in inlet flow temperature [17,29].

Referring to Fig. 12c, it is clear that bubbles waiting time declines as the inlet flow temperature increases. In fact, the higher the bulk temperature of the local liquid is, the shorter the time needed to recover the required superheat following a bubble departure is, which means faster bubble formation, i.e. lower waiting time [3,29,30].

Fig. 12d manifests nucleation frequencies versus inlet flow temperature. It can be seen that for higher inlet flow temperatures, bubbles depart with higher frequencies. This is attributable to the fact that higher inlet temperatures entails lower growth and waiting times as depicted in Figs. 12b and 12c.

3.4. Prediction of departure diameter and nucleation frequency

As mentioned earlier, accurate prediction of departure diameter and nucleation frequency brings about more reliable results in numerical simulations of sub-cooled flow boiling. Therefore, appropriate correlations are needed for these parameters. A number of correlations and models for departure diameter and nucleation frequency have been already proposed in the literature for various ranges of flow conditions and different working fluids in pool or flow boiling in straight channels. In the present section, the present data obtained from the U-shaped channel are predicted using these correlations to examine the ability of some common correlations and models proposed for pool or flow boiling in straight channels when predicting departure diameter and nucleation frequency in U-shaped channels. The results of these predictions are shown in Figs. 13a and 13b, respectively.

Journal Pre-proofs

The error analyses of predicting present data (departure diameter and nucleation frequency) using the existing correlations are presented in Tables 5a and 5b, respectively. The mean absolute deviation (MAD) and mean relative deviation (MRD) for departure diameter and nucleation frequency are defined as:

$$\mathrm{MAD}_{D_d} = \frac{1}{n}\sum_{i=1}^{n}\left|\frac{D_d(i)_{Pred} - D_d(i)_{exp}}{D_d(i)_{exp}}\right| \tag{4}$$

$$\mathrm{MAD}_{f_d} = \frac{1}{n}\sum_{i=1}^{n}\left|\frac{f_d(i)_{Pred} - f_d(i)_{exp}}{f_d(i)_{exp}}\right| \tag{5}$$

$$\mathrm{MRD}_{D_d} = \frac{1}{n}\sum_{i=1}^{n}\frac{D_d(i)_{Pred} - D_d(i)_{exp}}{D_d(i)_{exp}} \tag{6}$$

$$\mathrm{MRD}_{f_d} = \frac{1}{n}\sum_{i=1}^{n}\frac{f_d(i)_{Pred} - f_d(i)_{exp}}{f_d(i)_{exp}} \tag{7}$$

where $D_d(i)_{Pred}$ and $f_d(i)_{Pred}$ are respectively the predicted values of departure diameter and nucleation frequency for test i, while $D_d(i)_{exp}$ and $f_d(i)_{exp}$ denote the experimental values for test i, correspondingly. Also, n is the number of tests which is 68. As opposed to the MAD, the MRD is not a criterion of the accuracy of correlations and is used to check the degree of the over-prediction or under-prediction.

The significant deviations and errors shown in Figs. 13a and 13b and reported in Tables 5a and 5b can be attributable to the fact that the correlations and models employed in predicting present data have been developed for geometries other than curved channels and test conditions different from present ones. According to Holagh et al. [18], even under the same flow conditions and geometrical parameters (hydraulic diameter, channels cross-sectional shape, heating surface dimensions, site location, wall orientation and so forth), obtained values for the bubbles characteristics are completely different between a U-shaped channel and straight ones due to the presence of radial pressure gradient in the U-shaped channel. In essence, radial pressure gradient creates secondary flow in the U-shaped channel which plays a crucial role in liquid flow behavior surrounding the bubbles and subsequently, bubbles dynamic behavior and respective characteristics. In other words, the influence of radial pressure gradient on bubbles dynamic behavior must be taken into account when analyzing bubbles dynamic behavior and accordingly, predicting relevant

characteristics. On the other hand, the developed correlations and models for neither pool boiling nor flow boiling in straight channels take the impact of this phenomenon into consideration. Thus, it is expected and reasonable to encounter big errors when predicting bubbles characteristics in a U-shaped channel via correlations and models developed for pool boiling or flow boiling in straight channels.

3.5. Development of new correlations

Cooper et al. [44] presented a correlation for bubbles diameter based on Jakob and Boiling numbers, liquid-vapor density ratio, and the dimensionless sub-cooling temperature. These are considered as the four dimensionless parameters affecting bubbles diameter in straight channels [24]. Using suggestions made by Cooper et al. [44], Prodanovic et al. [24] presented a correlation for bubbles departure diameter during sub-cooled flow boiling in a straight vertical channel. The general form of this correlation is presented in Eq. (8),

$$D_d^+ = AJa^b\theta^c\left(\frac{\rho_l}{\rho_v}\right)^d Bo^e \tag{8}$$

where A, b, c, d, and e demonstrate empirical coefficients. Also, D_d^+, Ja, θ, $\frac{\rho_l}{\rho_v}$, and Bo are dimensionless departure diameter, Jakob number, dimensionless sub-cooling temperature, liquid-vapor phase density ratio, and Boiling number, respectively, defined as follows:

$$D_d^+ = \frac{D_d\sigma}{\rho_l\alpha_l^2} \tag{9}$$

$$Ja = \frac{\rho_l C_{pl}\Delta T_{sat}}{\rho_v h_{lv}} \tag{10}$$

$$\theta = \frac{T_w - T_b}{T_w - T_{sat}} \tag{11}$$

$$Bo = \frac{q''}{Gh_{lv}} \tag{12}$$

As previously mentioned and according to Abdous et al. [17] and Holagh et al. [18], in a U-shaped channel, radial pressure gradient has a huge part in the determination of bubbles dynamic behavior and respective characteristics. Thus, another appropriate dimensionless parameter as a representative of the influence of radial pressure gradient on bubbles departure diameter must be considered in Eq. (8) to harmonize it with bubbles departure diameter in a U-shaped channel. Dean

Journal Pre-proofs

number (De) is the only dimensionless parameter representing the curve geometry of the U-shaped channel, which is the root cause for the occurrence of radial pressure gradient. Therefore, the harmonized form of Eq. (8) with the U-shaped channel is as follows:

$$D_d^+ = AJa^b\theta^c\left(\frac{\rho_l}{\rho_v}\right)^d Bo^e De^f \tag{13}$$

$$De = Re\sqrt{\frac{D_H}{2R_c}} \tag{14}$$

where D_H and R_c are the channels hydraulic diameter and curvature radius, respectively.

Using Eq. (13) along with Eq. (16) which presents the dimensionless nucleation frequency, a new correlation for the prediction of dimensionless nucleation frequency can be developed as Eq. (16).

$$f_d^+ = f_d\frac{\rho_l^2\alpha_l^3}{\sigma^2} \tag{15}$$

$$f_d^+ (D_d^+)^2 = AJa^b\theta^c\left(\frac{\rho_l}{\rho_v}\right)^d Bo^e De^f \tag{16}$$

Applying the genetic algorithm to the experimental results (obtained from the tests introduced in Tables. 4a, 4b, and 4c), new correlations for the departure diameter and nucleation frequency based on the general forms of Eqs. (13) and (16) were obtained as follows:

$$D_d^+ = 71.73464 \times Ja^{8.7131}\theta^{2.4547}\left(\frac{\rho_l}{\rho_v}\right)^{-6.0301} Bo^{-4.1204} De^{-0.7629} \tag{17}$$

$$f_d^+ (D_d^+)^2 = 22.74518 \times Ja^{1.4811}\theta^{-1.3569}\left(\frac{\rho_l}{\rho_v}\right)^{1.7987} Bo^{1.6862} De^{0.3640} \tag{18}$$

As Figs. 14a and 14b show and reported in Tables 6a and 6b, Eq. (17) is able to predict present experimental departure diameters attained from S1 and S2 with MADs of 14.7% and 16.3%, respectively, while Eq. (18) is capable of estimating present experimental nucleation frequencies obtained from S1 and S2 with MADs of 8.4% and 22.7%, individually. To further assure that the proposed correlations take wall slope into account, the experimental results of Holagh et al. [18] obtained for the departure diameter and nucleation frequency of bubbles generating at three different locations inside a U-shaped channel with wall slopes of roughly 0°, 45°, and 90° were predicted using Eqs. (17) and (18). As can be seen in Figs. 14a and 14b, the predicted results are

Journal Pre-proofs

in good agreements with the experimental results of Holagh et al. [18]. On average, the two proposed correlations (Eqs. (17) and (18)) respectively have MADs of 18.0% and 18.5% when predicting departure diameter and nucleation frequency inside a U-shaped channel regarding all the available data. Detailed information on the error analysis of the proposed correlations for predicting present data and those reported by Holagh et al. [18] is provided in Tables 6a and 6b.

It is seen that the consideration of the influence of radial pressure gradient through adding De number as well as modifying the unknown parameters (A, b, c, d, e, and f) makes an enormous contribution to remarkable reductions in MAD when predicting relevant data inside a U-shaped channel. It is worth noting that these two newly developed correlations are applicable in U-shaped channels for the specified ranges of dimensionless numbers and flow conditions presented in Table 3.

4. Conclusions

In this study, bubbles departure characteristics, including departure diameter, growth and waiting times, and nucleation frequency were investigated in sub-cooled flow boiling of distilled water in a vertical U-shaped channel using high-speed photography. The effects of wall heat flux, mass flux, and inlet flow temperature on the mentioned characteristics were discussed. The obtained data for departure diameter and nucleation frequency were predicted utilizing some commonly used correlations and models developed for pool boiling and flow boiling in straight channels. Also, two new correlations were developed for predicting these characteristics in U-shaped channels which were in a good agreement with the present experimental data. The main outcomes of the current study are listed below.

- An increase in wall heat flux and inlet flow temperature and a decrease in mass flux result in larger bubble departure diameter and shorter waiting time, while bubbles growth time reduces as wall heat flux, mass flux, and inlet flow temperature rise.
- A drop in waiting time brings about higher bubble nucleation frequency as this parameter is the dominant factor in the determination of this parameter. Thus, an increase in wall heat flux, inlet flow temperature, and a reduction in mass flux leads to an escalation in the nucleation frequency.
- Correlations and models developed for bubbles departure diameter and nucleation frequency in pool boiling or flow boiling in straight channels are not able to accurately

predict experimental data in the vertical U-shaped channel. This is because these relations fail to consider the effect of radial pressure gradient as a result of the curved geometry in the U-shaped channel on bubbles dynamics behavior.

- Proposed correlation by Prodanovic et al. [24] was modified and adapted for predicting bubbles departure diameter and nucleation frequencies in U-shaped channels through adding Dean number as a new factor, which considers the influence of the curved geometry and subsequently, radial pressure gradient on bubbles characteristics.

Acknowledgements

We would like to sincerely thank Dr. Carlos A. Dorao (Department of Energy and Process Engineering, NTNU, Trondheim, Norway) for beneficial discussions.

Journal Pre-proofs

References

[1] Y.J. Cho, S.B. Yum, J.H. Lee, G.C. Park, Development of bubble departure and lift-off diameter models in low heat flux and low flow velocity conditions, Int. J. Heat Mass Transf. 54 (2011) 3234–3244. doi:10.1016/j.ijheatmasstransfer.2011.04.007.

[2] S.G. Holagh, M.A. Abdous, M. Shamsaiee, H. Saffari, Assessment of heat transfer enhancement technique in flow boiling conditions based on entropy generation analysis : twisted-tape tube, Heat Mass Transf. 56 (2020) 429–443. doi:https://doi.org/10.1007/s00231-019-02705-y.

[3] R. Sugrue, J. Buongiorno, T. McKrell, An experimental study of bubble departure diameter in subcooled flow boiling including the effects of orientation angle, subcooling, mass flux, heat flux, and pressure, Nucl. Eng. Des. 279 (2014) 182–188. doi:10.1016/j.nucengdes.2014.08.009.

[4] R. Sugrue, J. Buongiorno, A modified force-balance model for prediction of bubble departure diameter in subcooled flow boiling, Nucl. Eng. Des. 305 (2016) 717–722. doi:10.1016/j.nucengdes.2016.04.017.

[5] H.C. Ünal, Maximum bubble diameter, maximum bubble-growth time and bubble-growth rate during the subcooled nucleate flow boiling of water up to 17.7 MN/m2, Int. J. Heat Mass Transf. 19 (1976) 643–649. doi:10.1016/0017-9310(76)90047-8.

[6] T. Mazzocco, W. Ambrosini, R. Kommajosyula, E. Baglietto, A reassessed model for mechanistic prediction of bubble departure and lift off diameters, Int. J. Heat Mass Transf. 117 (2018) 119–124. doi:10.1016/j.ijheatmasstransfer.2017.09.105.

[7] S.C.P. Cheung, S. Vahaji, G.H. Yeoh, J.Y. Tu, Modeling subcooled flow boiling in vertical channels at low pressures – Part 1 : Assessment of empirical correlations, Int. J. Heat Mass Transf. (2014). doi:10.1016/j.ijheatmasstransfer.2014.03.016.

[8] N. Kurul, M.. Podowski, On the modeling of multi-dimensional effects in boiling channels, in: 27th Natl. Heat Transf. Conf., Minneapolis, 1991.

Journal Pre-proofs

[9] I.C. Chu, H.C. No, C.H. Song, Bubble lift-off diameter and nucleation frequency in vertical subcooled boiling flow, J. Nucl. Sci. Technol. 48 (2011) 936–949. doi:10.1080/18811248.2011.9711780.

[10] F.J. Collado, The law of stable equilibrium and the entropy-based boiling curve for flow boiling, Energy. 30 (2005) 807–819. doi:10.1016/j.energy.2004.04.007.

[11] V. Carey, Liquid Vapor Phase Change Phenomena, second, Taylor & Francis, 2008.

[12] S. Raj, M. Pathak, M.K. Khan, An analytical model for predicting growth rate and departure diameter of a bubble in subcooled flow boiling, Int. J. Heat Mass Transf. 109 (2017) 470–481. doi:10.1016/j.ijheatmasstransfer.2017.02.026.

[13] N. Zuber, The dynamics of vapor bubbles in nonuniform temperature fields, Int. J. Heat Mass Transf. 2 (1961) 83–98. doi:https://doi.org/10.1016/0017-9310(61)90016-3.

[14] M.G. Cooper, The microlayer and bubble growth in nucleate pool boiling, Int. J. Heat Mass Transf. 12 (1969) 915–933. doi:https://doi.org/10.1016/0017-9310(69)90155-0.

[15] M. Colombo, M. Fairweather, Prediction of bubble departure in forced convection boiling: A mechanistic model, Int. J. Heat Mass Transf. 85 (2015) 135–146. doi:10.1016/j.ijheatmasstransfer.2015.01.103.

[16] M.C. Vlachou, T.D. Karapantsios, Effect of channel inclination on heat transfer and bubble dynamics during subcooled flow boiling, Int. J. Therm. Sci. 124 (2018) 484–495. doi:10.1016/j.ijthermalsci.2017.10.041.

[17] M.A. Abdous, S.G. Holagh, M. Shamsaiee, H. Saffari, The prediction of bubble departure and lift-off radii in vertical U-shaped channel under subcooled flow boiling based on forces balance analysis, Int. J. Therm. Sci. 142 (2019) 316–331. doi:10.1016/j.ijthermalsci.2019.04.021.

[18] S.G. Holagh, M.A. Abdous, M. Shamsaiee, H. Sa, An experimental study on the influence of radial pressure gradient on bubbles dynamic behavior in subcooled flow boiling, Therm. Sci. Eng. Prog. 16 (2020). doi:10.1016/j.tsep.2019.100468.

[19] F. Ghunther, Photographic Study of Surface-Boiling Heat Transfer to Water Forced

Journal Pre-proofs

Convection, ASME J. Heat Transf. 73 (1951) 115–123.

[20] V. Tolubinsky, D. Kostanchuk, Vapour bubbles growth rate and heat transfer intensity at subcooled water boiling, in: Fourth Int. Heat Transf. Conf., Paris, 1970.

[21] A.H. Abdelmessih, F.C. Hooper, S. Nangia, Flow effects on bubble growth and collapse in surface boiling, Int. J. Heat Mass Transf. 15 (1972) 115–125. doi:10.1016/0017-9310(72)90170-6.

[22] J.F. Klausner, R. Mei, D.M. Bernhard, L.Z. Zeng, Vapor bubble departure in forced convection boiling, Int. J. Heat Mass Transf. 36 (1993) 651–662. doi:10.1016/0017-9310(93)80041-R.

[23] G.E. Thorncroft, J.F. Klausner, R. Mei, An experimental investigation of bubble growth and detachment in vertical upflow and downflow boiling, Int. J. Heat Mass Transf. 41 (1998) 3857–3871. doi:10.1016/S0017-9310(98)00092-1.

[24] V. Prodanovic, D. Fraser, M. Salcudean, Bubble behavior in subcooled flow boiling of water at low pressures and low flow rates, Int. J. Multiph. Flow. 28 (2002) 1–19. doi:10.1016/S0301-9322(01)00058-1.

[25] C. Morel, M. Stephane, M. Jerome, B. Marc, R113 boiling bubbly flow in an annular geometry simulated with the NEPTUNE code, in: 11th Int. Top. Meet. Nucl. React. Therm. Hydraul., 2005.

[26] N. Basu, G.R. Warrier, V.K. Dhir, Wall Heat Flux Partitioning During Subcooled Flow Boiling: Part 1—Model Development, J. Heat Transfer. 127 (2005) 131. doi:10.1115/1.1842784.

[27] L. Zou, B.G. Jones, Heating surface material's effect on subcooled flow boiling heat transfer of R134a, Int. J. Heat Mass Transf. 58 (2013) 168–174. doi:10.1016/j.ijheatmasstransfer.2012.11.036.

[28] P. Guan, L. Jia, L. Yin, Z. Tan, Bubble departure size in flow boiling, Heat Mass Transf. 51.7 (2015) 921–930. doi:10.1007/s00231-014-1461-7.

[29] C. Brooks, N. as Silin, T. Hibiki, M. Ishii, Experimental Investigation of Wall Nucleation

Journal Pre-proofs

Characteristics in Flow Boiling, J. Heat Transfer. 137 (2015) 1–9. doi:10.1115/1.4029593.

[30] P. Goel, A.K. Nayak, P. Ghosh, J.B. Joshi, Experimental study of bubble departure characteristics in forced convective subcooled nucleate boiling, Exp. Heat Transf. 00 (2017) 1–25. doi:10.1080/08916152.2017.1397821.

[31] Z.J. Ooi, V. Kumar, J.L. Bottini, C.S. Brooks, Experimental investigation of variability in bubble departure characteristics between nucleation sites in subcooled boiling flow, Int. J. Heat Mass Transf. 118 (2018) 327–339. doi:10.1016/j.ijheatmasstransfer.2017.10.116.

[32] N. Colgan, J.L. Bottini, Z.J. Ooi, C.S. Brooks, Experimental study of wall nucleation characteristics in flow boiling under subatmospheric pressures in a vertical square channel, Int. J. Heat Mass Transf. 134 (2019) 58–68. doi:10.1016/j.ijheatmasstransfer.2018.12.153.

[33] P. Zhou, R. Huang, S. Huang, Y. Zhang, X. Rao, Experimental investigation on bubble contact diameter and bubble departure diameter in horizontal subcooled flow boiling, Int. J. Heat Mass Transf. 149 (2019) 119105. doi:10.1016/j.ijheatmasstransfer.2019.119105.

[34] T. Ren, Z. Zhu, M. Yan, J. Shi, C. Yan, Experimental study on bubble nucleation and departure for subcooled flow boiling in a narrow rectangular channel, Int. J. Heat Mass Transf. 144 (2019) 118670. doi:10.1016/j.ijheatmasstransfer.2019.118670.

[35] R. Cole, Photographic Study of Pool Boiling in the Region of Critical Heat Flux, AIChE J. 6 (1960) 533–538. doi:10.1002/aic.690060405.

[36] N. Zuber, Nucleate boiling. The region of isolated bubbles and the similarity with natural convection, Int. J. Heat Mass Transf. 6 (1962) 53–78. doi:10.1016/0017-9310(63)90029-2.

[37] A.. Hatton, I.. Hall, Photographic study of boiling on prepared surfaces, in: Third Int. Heat Transf. Conf., Illinois, 1966: pp. 24–37.

[38] H. Ivey, Relationship between bubble frequency,departure diameter and rise velocity in nucleate boiling, Int. J. Heat Mass Transf. 10 (1967) 1023–1040. doi:https://doi.org/10.1016/0017-9310(67)90118-4.

[39] L.Z. Zeng, J.F. Klausner, R. Mei, A unified model for the prediction of bubble detachment

Journal Pre-proofs

diameters in boiling systems—II. flow boiling, Int. J. Heat Mass Transf. 36 (1993) 2261–2270. doi:10.1016/S0017-9310(05)80112-7.

[40] R. Situ, M. Ishii, T. Hibiki, J.Y. Tu, G.H. Yeoh, M. Mori, Bubble departure frequency in forced convective subcooled boiling flow, Int. J. Heat Mass Transf. 51 (2008) 6268–6282. doi:10.1016/j.ijheatmasstransfer.2008.04.028.

[41] D. Euh, B. Ozar, T. Hibiki, M. Ishii, C. Song, Characteristics of Bubble Departure Frequency in a Low-Pressure Subcooled Boiling Flow Characteristics of Bubble Departure Frequency, J. Nucl. Sci. Technol. 3131 (2012) 1881–1248. doi:10.1080/18811248.2010.9720958.

[42] R. Situ, T. Hibiki, M. Ishii, M. Mori, Bubble lift-off size in forced convective subcooled boiling flow, Int. J. Heat Mass Transf. 48 (2005) 5536–5548. doi:10.1016/j.ijheatmasstransfer.2005.06.031.

[43] B.G. Suhas, A. Sathyabhama, Bubble dynamics of water-ethanol mixture during subcooled flow boiling in a conventional channel, Appl. Therm. Eng. 113 (2017) 1596–1609. doi:10.1016/j.applthermaleng.2016.11.126.

[44] M.G. Cooper, K. Mori, C.R. Stone, behavior of vapor bubble growing at a wall with force flow, Int. J. Heat Mass Transf. 26 (1983) 1489–1707. doi:https://doi.org/10.1016/S0017-9310(83)80049-0.

Journal Pre-proofs

Nomenclature		**Greek symbols**	
D_d	Departure diameter (mm)	ρ	Density ($kg.m^{-3}$)
f_d	Nucleation frequency (s^{-1})	θ	Dimensionless sub-cooling
t_g	Growth time (ms)	σ	Surface tension (Nm^{-1})
t_w	Waiting time (ms)	α	Thermal diffusivity (m^2s^{-1})
D_H	Channel hydraulic diameter (mm)	ΔT_{sat}	Wall superheat (˚C)
R_c	Channel curvature radius	**Subscripts**	
u_l	Flow velocity (ms^{-1})	d	Departure
h_{lv}	Enthalpy of vaporization ($kJ.kg^{-1}$)	g	Growth
c_p	Heat capacity ($kJ.kg^{-1}K^{-1}$)	l	Liquid phase
q''	Wall heat flux ($kW.m^{-2}$)	v	Vapor phase
P	Pressure (bar)	w	Waiting
T	Temperature (˚C)	W	Wall
G	Mass flux ($kg.m^{-2}s^{-1}$)	b	Bulk
Ja	Jakob number	In	Inlet
Bo	Boiling number	out	Outlet
De	Dean number		
Re	Reynolds number		

Journal Pre-proofs

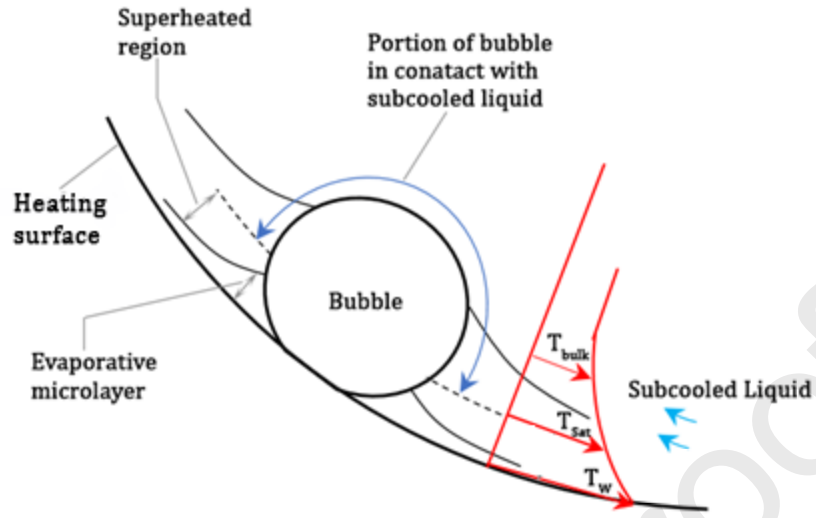

Fig. 1: Schematic of different liquid layers surrounding a bubble in subcooled boiling flow, adopted from [12]

Journal Pre-proofs

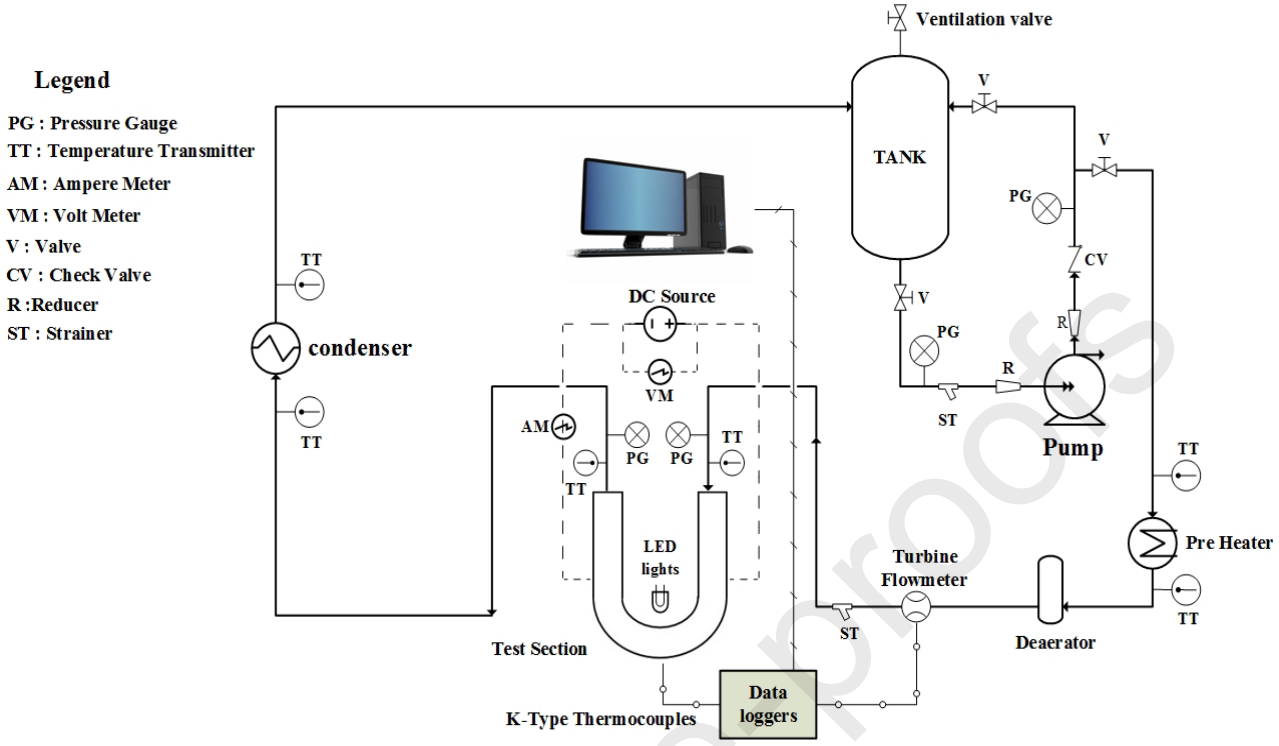

Fig. 2: Schematic diagram of the test rig

Journal Pre-proofs

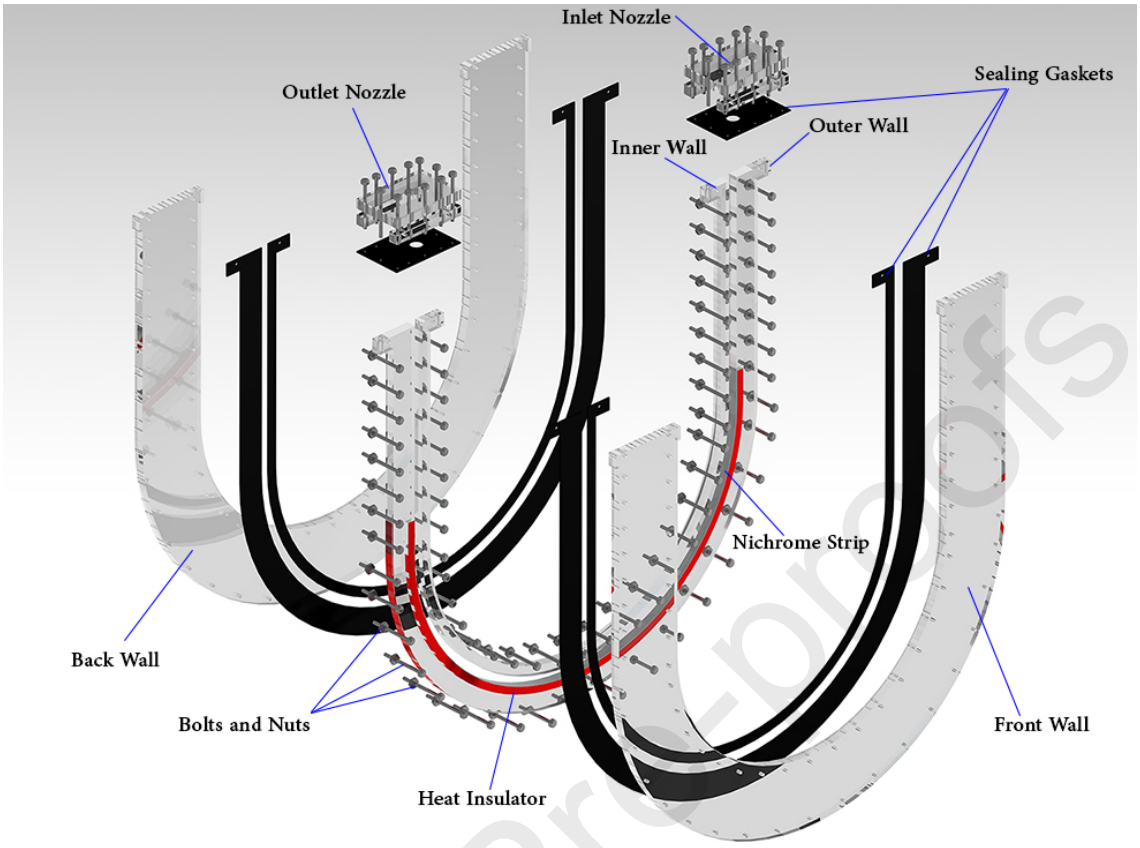

Fig. 3: Schematic of the test section assembly

Journal Pre-proofs

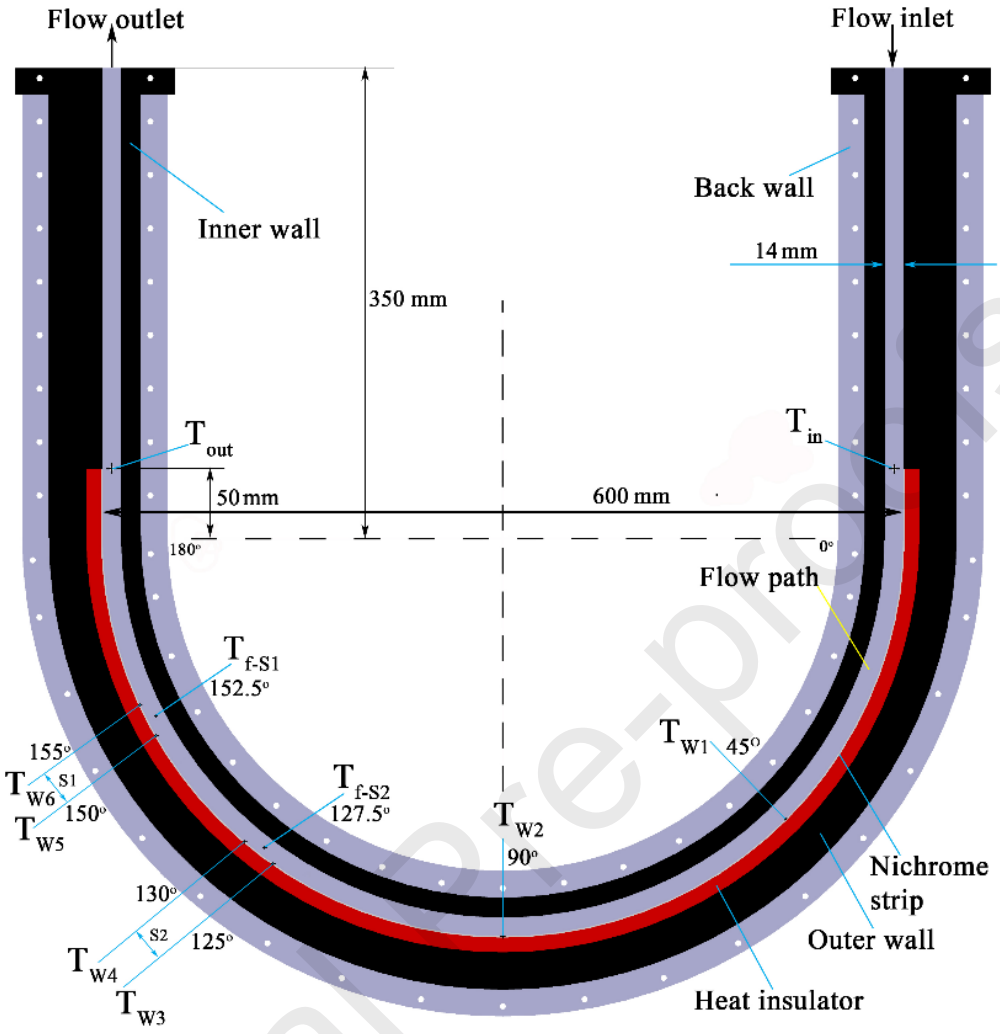

Fig. 4a: Thermocouples locations and important dimensions

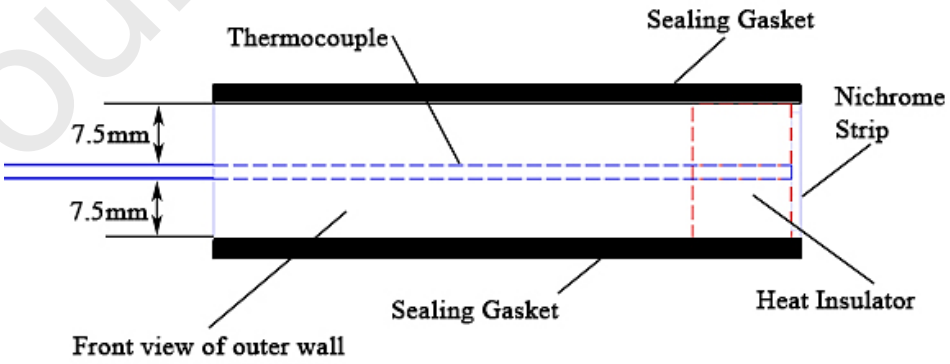

Fig. 4b: Thermocouple installation behind the Nichrome strip

Journal Pre-proofs

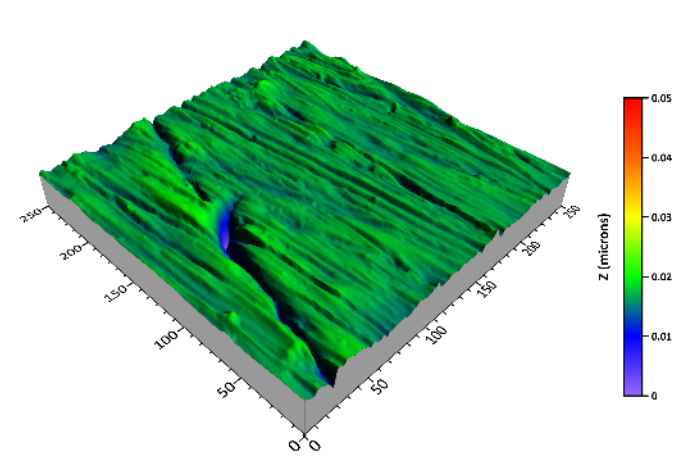

(a)

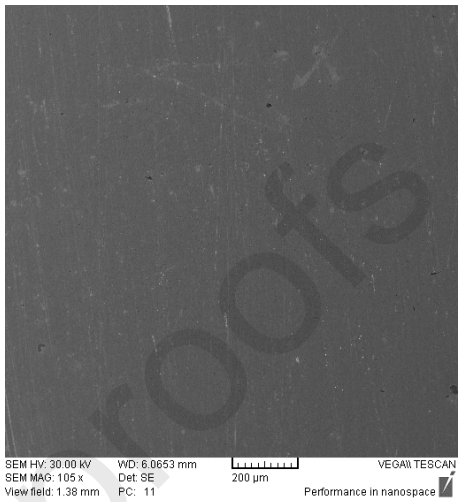

(b)

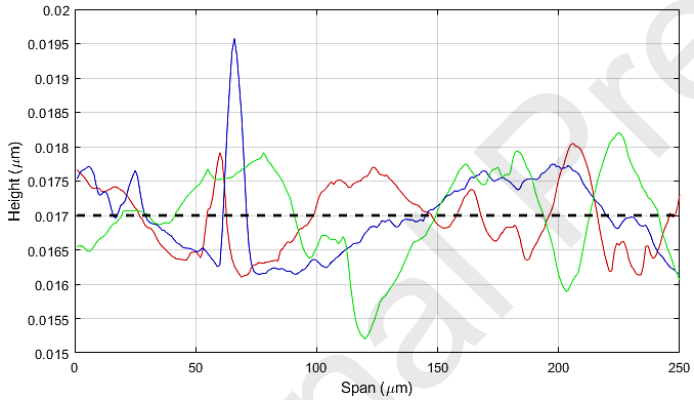

(c)

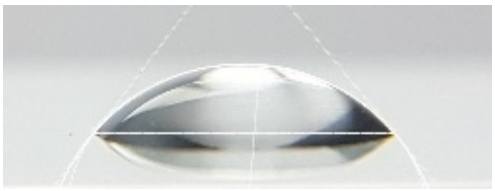

(d)

Fig. 5: The visual Outputs of (a) AFM and (b) SEM (c) Surface sample profiles (d) droplet contact angle

Journal Pre-proofs

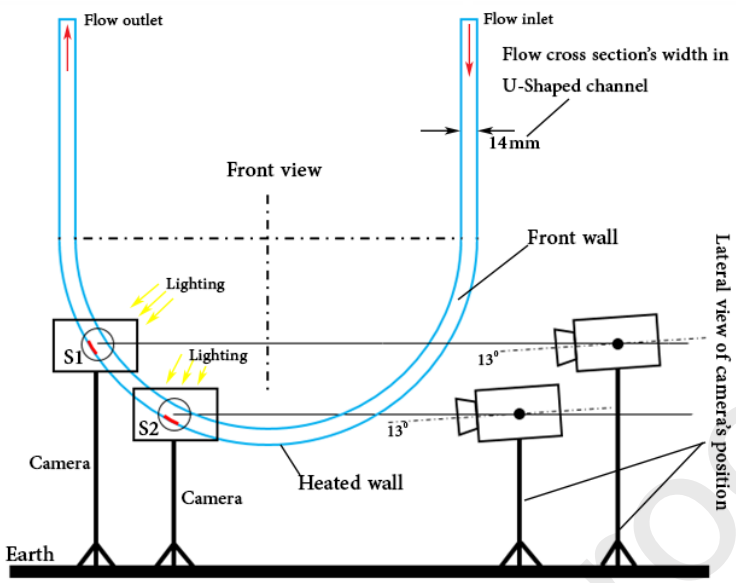

Fig. 6: The position of the camera against the U-shaped channel

Journal Pre-proofs

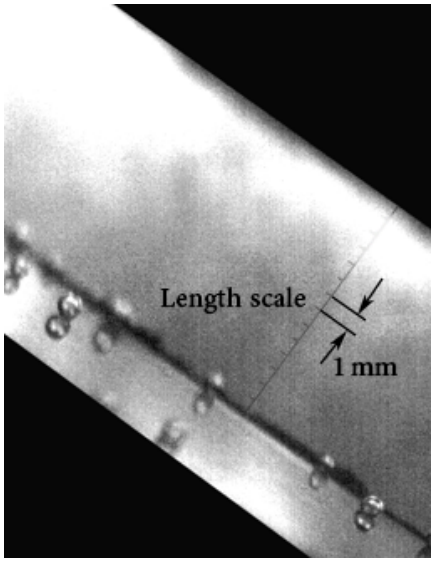

Fig. 7: Considered length scale in image processing (measurement ruler)

Journal Pre-proofs

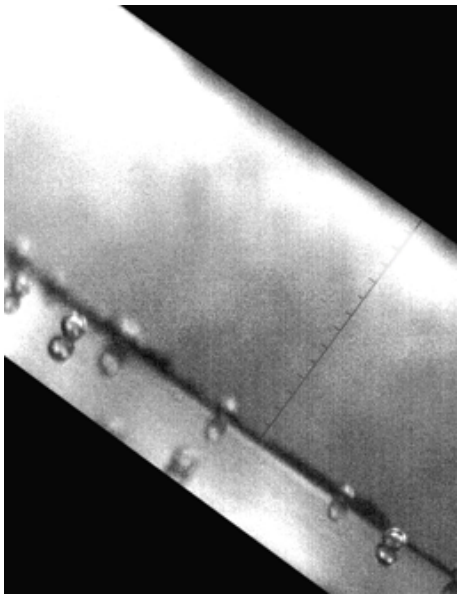

(a)

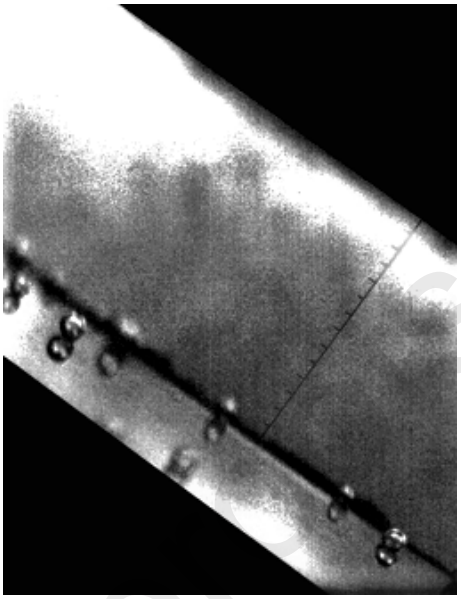

(b)

(c)

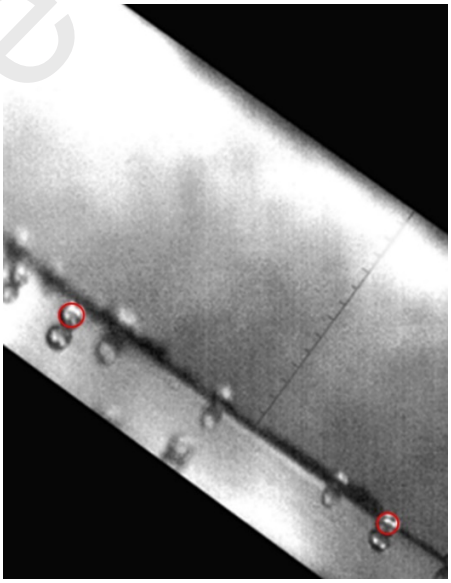

(d)

Journal Pre-proofs

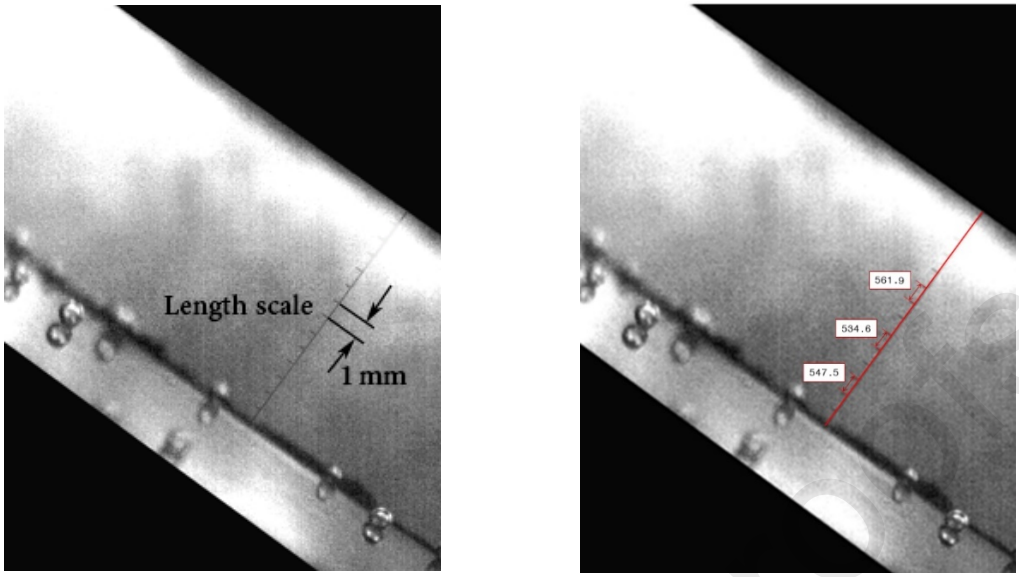

(e) **(f)**

Fig. 8: (a) The original image, (b) the enhanced version, (c) the detected background (d) the result of bubble detection code, (e) the length of the engraved marks in millimeters, and (f) the length of the engraved marks in pixels

Journal Pre-proofs

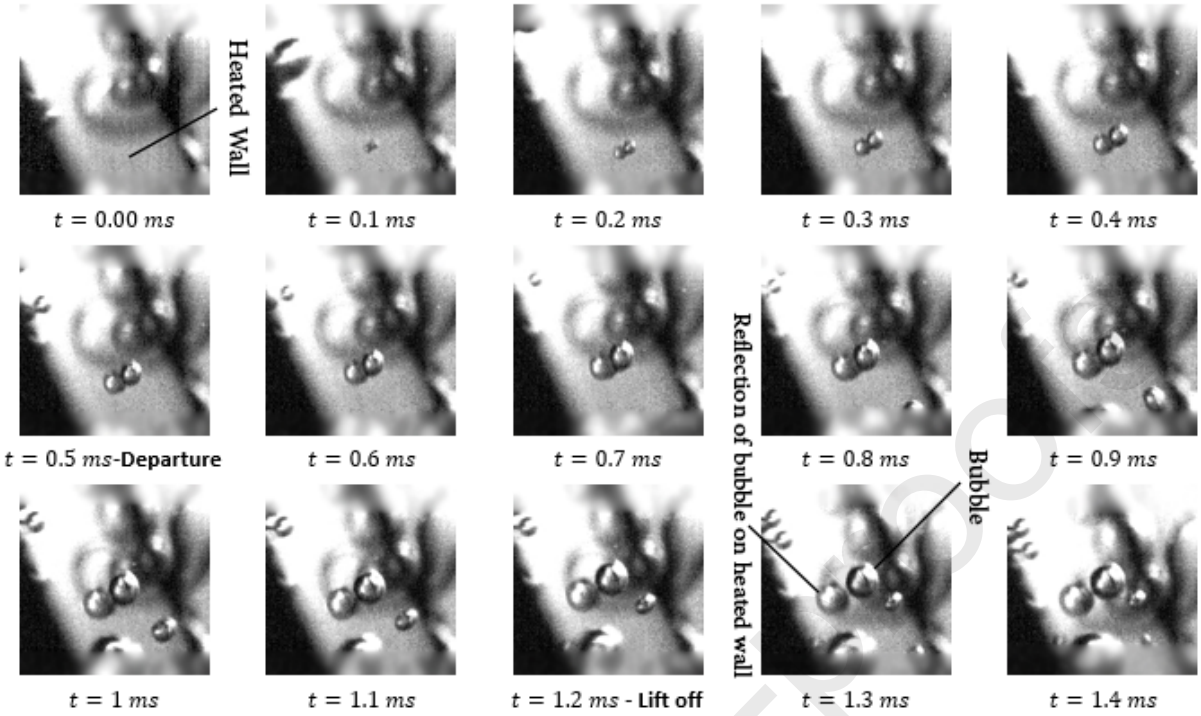

Fig. 9: Typical successive images of bubbles forming, growth, departure, slip and lift off for experiment number HFE1-S1-4

Journal Pre-proofs

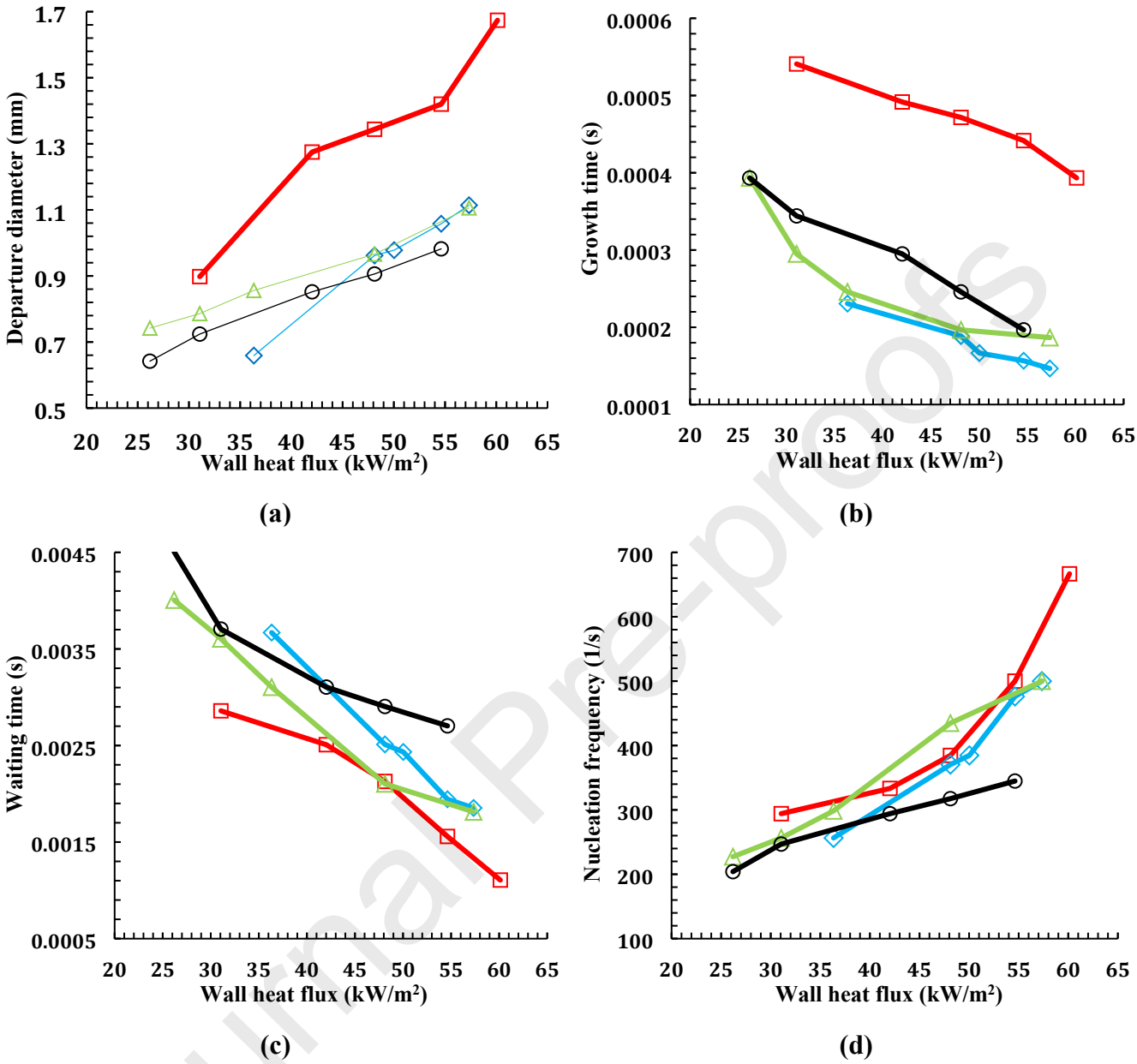

Flow conditions		site	Test Group
T_{in}(°C)	G(kg.m^{-2}.s^{-1})		
93.6	127.4	S1	HFE1-S1
94.5	222.9	S1	HFE2-S1
94.7	159.2	S2	HFE3-S2
95.2	191.1	S2	HFE4-S2

Fig. 10: The influence of variation in wall heat flux on (a) departure diameter, (b) growth time, (c) waiting time, and (d) nucleation frequency (Table 4a)

Journal Pre-proofs

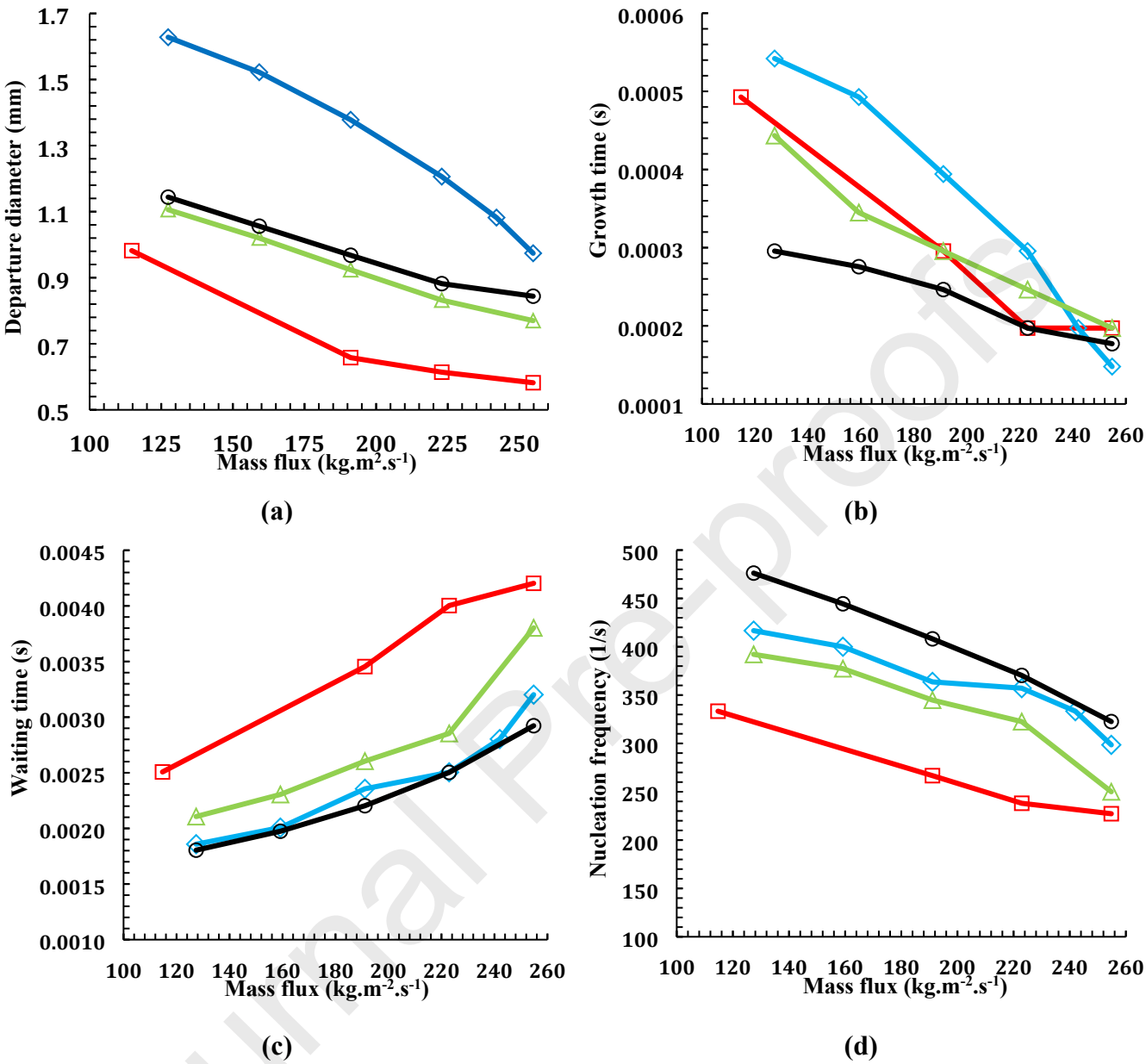

	Flow conditions		site	Test Group
	T_{in}(℃)	q″(kW.m^{-2})		
□	94.3	36.334	S1	FVE1-S1
◇	95.7	50.027	S1	FVE2-S1
△	95.5	42.021	S2	FVE3-S2
○	95.0	54.624	S2	FVE4-S2

Fig. 11: The influence of variation in mass flux on (a) departure diameter, (b) growth time, (c) waiting time, and (d) nucleation frequency (Table 4b)

Journal Pre-proofs

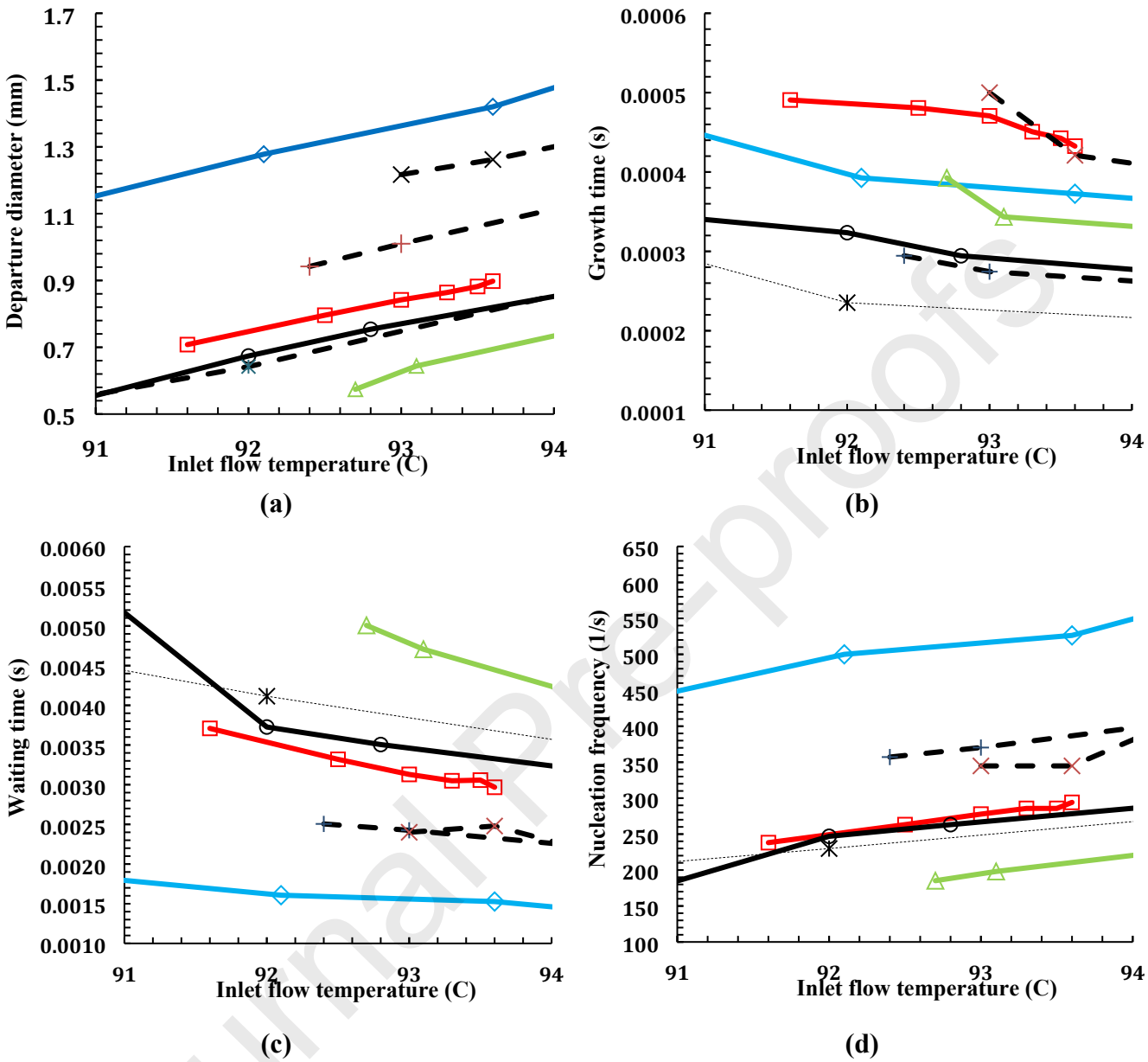

t_g	Flow conditions		site	Test Group
	G(kg.m^{-2}.s^{-1})	q″(kW.m^{-2})		
□	127.4	31.056	S1	SEF1-S1
✕	159.2	48.118	S1	SEF2-S1
◇	127.4	54.624	S1	SEF3-S1
△	127.4	26.187	S2	SEF4-S2
○	127.4	36.334	S2	SEF5-S2
+	127.4	42.021	S2	SEF6-S2
✳	159.2	42.021	S2	SEF7-S2

Fig. 12: The influence of variation in inlet flow temperature on (a) departure diameter, (b) growth time, (c) waiting time, and (d) nucleation frequency (Table 4c)

Journal Pre-proofs

(a)

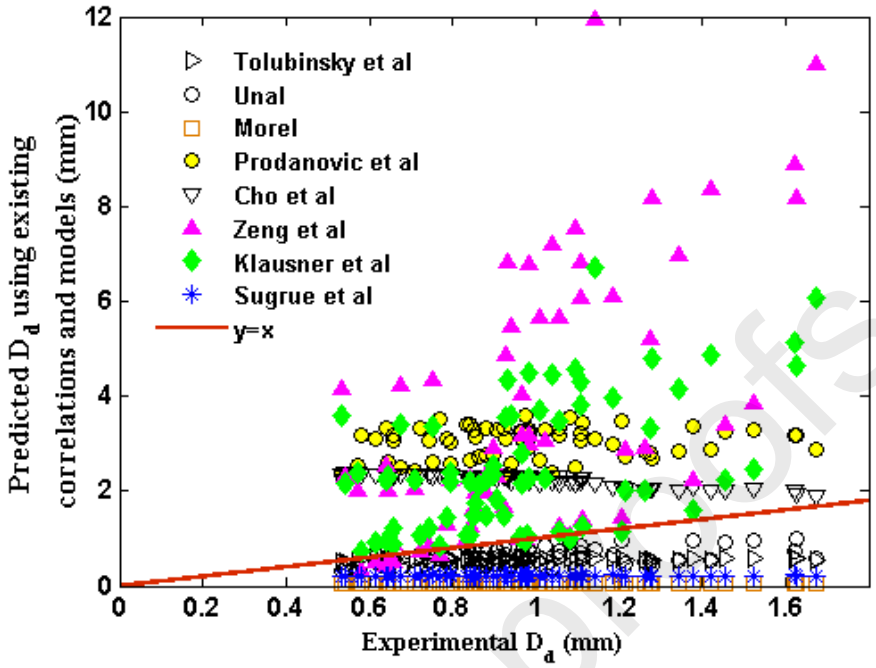

(b)

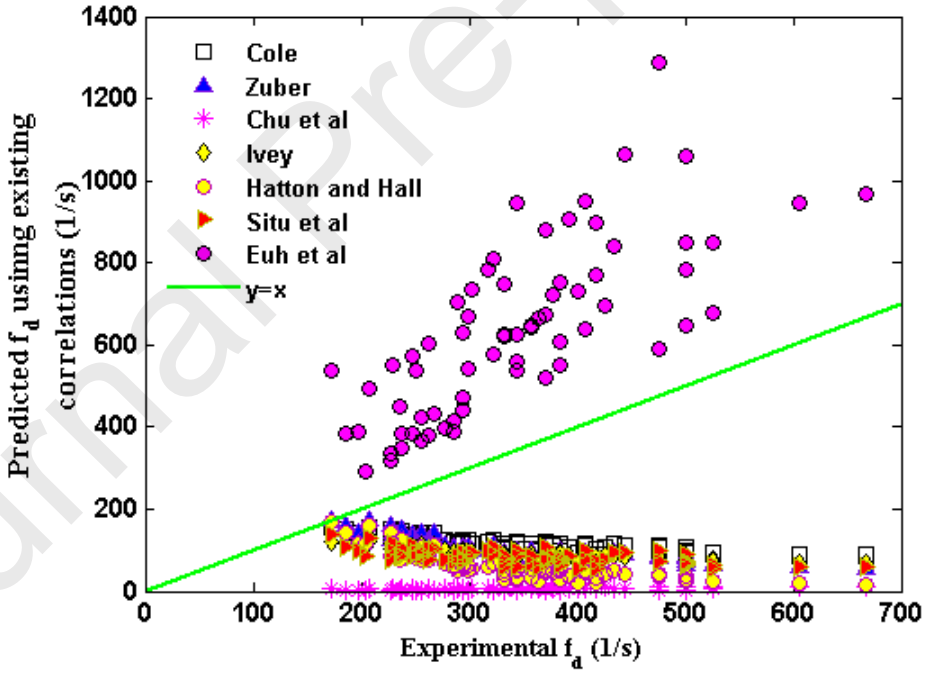

Fig. 13: Evaluation of the accuracy of correlations and models developed for (a) departure diameter and (b) nucleation frequency in pool boiling and flow boiling in straight channels when predicting present experimental data

Journal Pre-proofs

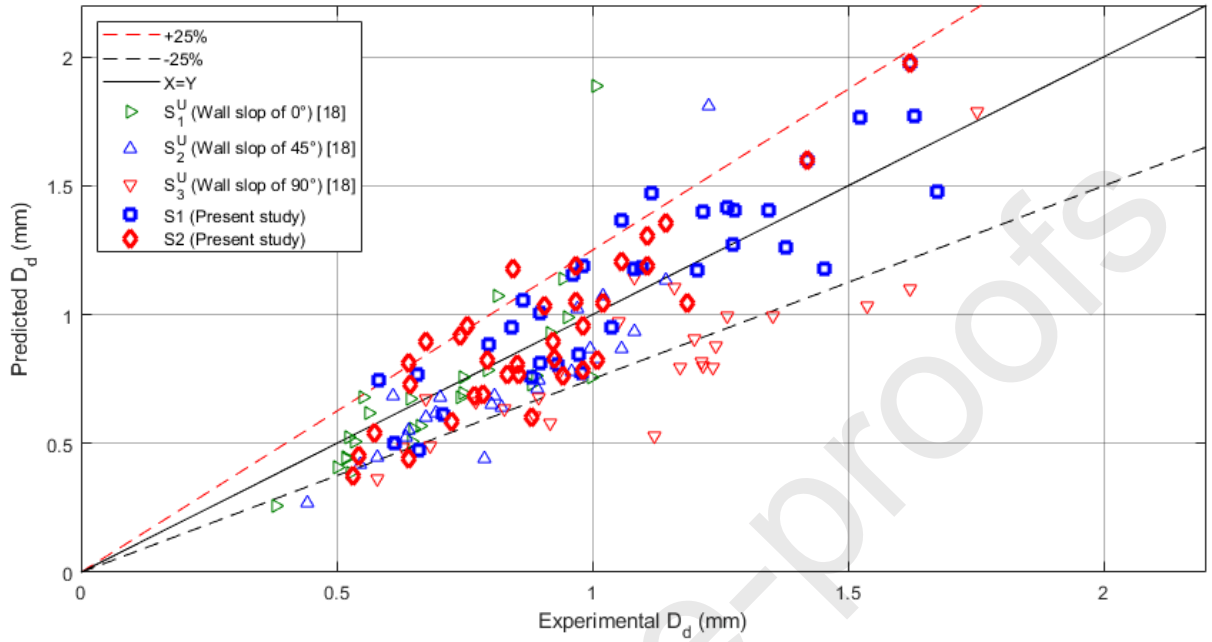

Fig. 14a: Comparison between predicted (by Eq. (17)) and measured (present experiments and those conducted by Holagh et al. [18]) bubble departure diameters

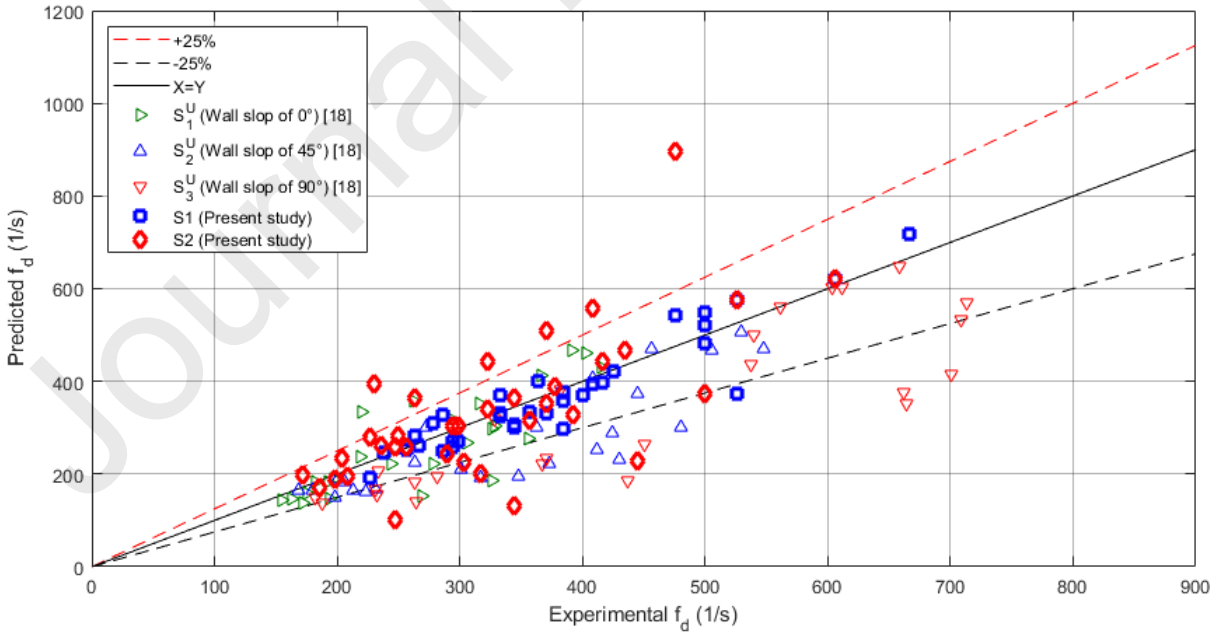

Fig. 14b: Comparison between predicted (by Eq. (18)) and measured (present experiments and those conducted by Holagh et al. [18]) bubble nucleation frequencies

Journal Pre-proofs

Table 1a: Summary of some existing studies on bubbles dynamic behavior in in the literature

Study	fluid	Geometry	D_H (mm)	Orientation	Heating surface	Date points	$q''(\frac{kW}{m^2})$	$G\ (\frac{kg}{m^2 s^1})$	$\Delta T_{sub}(°C)$	P (bar)	D_d	D_{lo}	f_d
Ghunther [19]	Water	Rectangular	-	Horizontal	Stainless steel	38	4500-6140	77-6088	20-86	1-1.7	●		
Tolubinsky and Kostanchuk [20]	Water	Rectangular	-	Horizontal	Stainless steel	5	470	192-198	5-60	1	●		
Abdelmessih et al. [21]	Water	Annular	-	Horizontal	Stainless steel	34	187-460	796-1274	1.85	1	●		●
Ünal [5]	Water	Annular	-	Horizontal	Stainless steel	7	380-550	3100-3600	3-6	139-177	●		●
Klausner et al. [22]	R-113	Rectangular	25	Horizontal	Nichrome	35	11-26	112-287	Saturated	1	●		
Thorncroft et al. [23]	FC-87	Square	12.7	Vertical	Nichrome	20	1.3-14.6	192-666	1.9-5	1	●	●	●
Prodanovic et al. [24]	Water	Annular	9.3	Vertical	Stainless steel	54	200-1000	76-766	10-30	1-3	●	●	
Situ et al. [42]	Water	Annular	19.1	Vertical	Stainless steel	91	54-206	466-900	2-20	1		●	
Situ et al. [40]	Water	Annular	19.1	Vertical	Stainless steel	58	60.7-206	478-905	1.5-20	1		●	
Cho et al. [1]	Water	Rectangular	-	Vertical	Copper	17	2.7-6.5	20.7-47.2	2.1-11.8	1	●	●	
Chu et al. [9]	Water	Annular	22.2	Vertical	NCF 600	14	140-200	300-700	3.4-22.6	1.3-1.5		●	●
Euh et al. [41]	Water	Annular	40.4	Vertical	Stainless steel	76	61-238	214-1869	7.5-23.4	1.7-3.5			●
Zou and Jones [27]	R-134a	Square	12.7	Horizontal	Stainless steel and Copper	48	0-630	63-378	10-30	4.5-8	●		
Sugrue et al. [3]	Water	Rectangular	16.7	$0° - 180°$	Stainless steel	64	50-100	250-400	10-20	1-5	●		
Guan et al.[28]	Water	Annular	5.1	Vertical	Stainless steel	12	68.2-101.4	87-319	8.5-10.5	1	●		
Brooks et al. [29]	Water	Annular	19.1	Vertical	Stainless steel	83	100-492	235-986	5-40	1.5-3	●		●
Goel et al. [30]	Water	Annular	33	Vertical	Stainless steel	42	52.6-95.5	6.6-13.3	10-30	1	●	●	●
Ooi et al. [31]	Water	Square	12.7	Vertical	Copper	9	231-295	260-422	12.1-24.3	1.4-4.4	●		●
Vlachou and Karapantsios [16]	Water	Rectangular	16	$0° - 150°$	Copper	-	200-1000	330-830	70	1	●		●
Zhou et al. [33]	Water	Rectangular	19.8	Horizontal	Aluminum	34	231-550	949-1928	7-14	1.2-2.3	●		
Ren et al. [34]	Water	Rectangular	3.8	Vertical	Stainless steel	58	100-700	300-1700	20-50	0.2-0.6	●		
Abdous et al. [17]	Water	Rectangular	15.7	U-shaped	Nichrome	68	26.1-61.5	114-255	1-8	1	●	●	
Holagh et al. [18]	Water	Rectangular	15.7	U-shaped and straight	Nichrome	25	36.3-54.6	129.3-260	1.7-5.7	1	●	●	●

Journal Pre-proofs

Journal Pre-proofs

Table 1b: Reported ranges for bubbles characteristics in the literature

Study	D_d(mm)	D_{lo}(mm)	t_d(ms)	t_{lo}(ms)	t_w(ms)	$f_d(s^{-1})$
Ghunther [19]	0.32-1.02		0.8-3			
Tolubinsky and Kostanchuk [20]	0.47-1.24		1.2			
Ünal [5]	0.11-0.18					
Klausner et al. [22]	0.1-0.65					
Thorncroft et al. [23]	0.09-0.25	0.12-45	1-1.8		17-30	
Prodanovic et al. [24]	0.3-2.68	0.37-2.86	0.41-9.5	0.81-18.6		
Situ et al.[42]		0.145-0.6				
Cho et al. [1]	0.46-0.56	0.55-0.9				
Chu et al. [9]		0.51-1.71				77-300
Euh et al.[41]						20-900
Zou and Jones [27]	0.15-0.45					
Sugrue et al. [3]	0.22-0.66					
Guan et al. [28]	0.62-1.85					
Brooks et al. [29]	0.05-0.3					120-1450
Goel et al. [30]	0.31-0.58	0.31-0.96	3-7		22-90	10-41
Ooi et al. [31]	0.2-0.5					10-600
Vlachou and Karapantsios [16]	0.02-0.66					
Zhou et al. [33]	0.21-0.31					
Ren et al. [34]	0.01-0.78					
Abdous et al [17]	0.53-1.67	0.82-2.4				
Holagh et al [18] (for straight channel)	0.21-0.78	0.35-1.25	0.35-0.95	1.6-3.45	2.3-8.5	110-355
Holagh et al [18] (for U-shaped channel)	0.38-1.75	0.52-1.98	0.15-0.65	0.45-1.65	1-6.1	150-715

Journal Pre-proofs

Table 2: Accuracy of instruments and uncertainty analysis

Instrument type	unit	Accuracy	Objective function	unit	Uncertainty
Temperature Transmitter	℃	0.1	$A_{\text{cross section}}$	mm^2	0.456
Thermocouples	℃	0.1	$A_{\text{Nichrome strip}}$	mm^2	19.891
Pressure gage	bar	0.05	Electrical power	W/m^2	2.58-4.1
Flow meter	L/min	3% full scale-read	Heat flux	kW/m^2	0.216-0.35
Ampere meter	A	0.5	Bubble diameter	mm	0.0364
Volt meter	V	0.01	Growth time	ms	0.05

Journal Pre-proofs

Table 3. General ranges of the experiments

Parameter	Value
P (bar)	Atmospheric
$T_{sat}(°C)$	96.7
$T_{in}(°C)$	88.7-95.7
$\Delta T_{sub}(°C)$	1-8
$\Delta P_R(Pa)$	0.81-3.29
$u_l\ (m.s^{-1})$	0.132-0.265
$G\ (kg.m^{-2}s^{-1})$	114-255
$q''(kW.m^{-2})$	26.1-61.5
Ja	9.4-19.9
Bo $(\times 10^{-5})$	6.2-21.3
Re	6217-13630
De	970-2220

Journal Pre-proofs

Table 4a. Test matrix (heat flux variation)

Test Group	Test Case	T_{in}(℃)	$G\left(\frac{kg}{m^2.s}\right)$	$q''(\frac{kW}{m^2})$
HFE1-S1	HFE1-S1-1	93.6	127.4	31.056
	HFE1-S1-2	93.6	127.4	42.021
	HFE1-S1-3	93.6	127.4	48.118
	HFE1-S1-4	93.6	127.4	54.624
	HFE1-S1-5	93.6	127.4	60.123
HFE2-S1	HFE2-S1-1	94.5	222.9	36.334
	HFE2-S1-2	94.5	222.9	48.118
	HFE2-S1-3	94.5	222.9	50.027
	HFE2-S1-4	94.5	222.9	54.624
	HFE2-S1-5	94.5	222.9	57.340
HFE3-S2	HFE3-S2-1	94.7	159.2	26.187
	HFE3-S2-2	94.7	159.2	31.056
	HFE3-S2-3	94.7	159.2	36.334
	HFE3-S2-4	94.7	159.2	48.118
	HFE3-S2-5	94.7	159.2	57.340
HFE4-S2	HFE4-S2-1	95.2	191.1	26.187
	HFE4-S2-2	95.2	191.1	31.056
	HFE4-S2-3	95.2	191.1	42.021
	HFE4-S2-4	95.2	191.1	48.118
	HFE4-S2-5	95.2	191.1	54.624

Table 4b. Test matrix (mass flux variation)

Test Group	Test Case	T_{in}(℃)	$G\left(\frac{kg}{m^2.s}\right)$	$q''(\frac{kW}{m^2})$
FVE1-S1	FVE1-S1-1	94.3	114.7	36.334
	FVE1-S1-2	94.3	191.1	36.334
	FVE1-S1-3	94.3	222.9	36.334
	FVE1-S1-4	94.3	254.8	36.334
FVE2-S1	FVE2-S1-1	95.7	127.4	50.027
	FVE2-S1-2	95.7	159.2	50.027
	FVE2-S1-3	95.7	191.1	50.027
	FVE2-S1-4	95.7	222.9	50.027
	FVE2-S1-5	95.7	242.0	50.027
	FVE2-S1-6	95.7	254.8	50.027
FVE3-S2	FVE3-S2-1	95.5	127.4	42.021
	FVE3-S2-2	95.5	159.2	42.021
	FVE3-S2-3	95.5	191.1	42.021
	FVE3-S2-4	95.5	222.9	42.021
	FVE3-S2-5	95.5	254.8	42.021
FVE4-S2	FVE4-S2-1	95.0	127.4	54.624
	FVE4-S2-2	95.0	159.2	54.624
	FVE4-S2-3	95.0	191.1	54.624
	FVE4-S2-4	95.0	222.9	54.624
	FVE4-S2-5	95.0	254.8	54.624

Table 4c. Test matrix (inlet flow temperature variation)

Test Group	Test Case	T_{in}(℃)	$G\left(\frac{kg}{m^2.s}\right)$	$q''(\frac{kW}{m^2})$	Test Group	Test case	T_{in}(℃)	$G\left(\frac{kg}{m^2.s}\right)$	$q''(\frac{kW}{m^2})$
SEF1-S1	SEF1-S1-1	91.6	127.4	31.056	SEF4-S2	SEF4-S2-1	92.7	127.4	26.187
	SEF1-S1-2	92.5	127.4	31.056		SEF4-S2-2	93.1	127.4	26.187
	SEF1-S1-3	93.0	127.4	31.056		SEF4-S2-3	94.6	127.4	26.187
	SEF1-S1-4	93.3	127.4	31.056	SEF5-S2	SEF5-S2-1	90.8	127.4	36.334
	SEF1-S1-5	93.5	127.4	31.056		SEF5-S2-2	92	127.4	36.334
	SEF1-S1-6	93.6	127.4	31.056		SEF5-S2-3	92.8	127.4	36.334
SEF2-S1	SEF2-S1-1	93.0	159.2	48.118		SEF5-S2-4	94.9	127.4	36.334
	SEF2-S1-2	93.6	159.2	48.118	SEF6-S2	SEF6-S2-1	92.4	127.4	42.021
	SEF2-S1-3	95.6	159.2	48.118		SEF6-S2-2	93	127.4	42.021
SEF3-S1	SEF3-S1-1	88.7	127.4	54.624		SEF6-S2-3	94.7	127.4	42.021
	SEF3-S1-2	89.6	127.4	54.624	SEF7-S2	SEF7-S2-1	90.8	159.2	42.021
	SEF3-S1-3	90.5	127.4	54.624		SEF7-S2-2	92	159.2	42.021
	SEF3-S1-4	92.1	127.4	54.624		SEF7-S2-3	95.2	159.2	42.021
	SEF3-S1-5	93.6	127.4	54.624					
	SEF3-S1-6	95.0	127.4	54.624					

Journal Pre-proofs

Table 5a. Prediction accuracy of existing departure diameter correlations and models

Departure diameter correlations and models	All data (%)		Percentile of data in given error bands (%)				
	MAD	MRD	± 10%	± 20%	± 30%	± 40%	± 50%
Tolubinsky and Kostanchuk [20]	37.9	-37.9	8.8	20.0	31.6	48.5	75
Ünal [5]	36.9	-36.8	5.8	22.0	33.8	58.8	73.5
Morel et al. [25]	93.4	-93.4	0.0	0.0	0.0	0.0	0.0
Prodanovic et al. [24]	227.6	227.6	0.0	0.0	0.0	0.0	0.0
Cho et al. [1]	148.9	148.9	0.0	2.9	4.4	7.3	10.3
Zeng et al. [39]	252.8	248.8	5.9	14.7	20.6	22.0	23.5
Klausner et al. [22]	165.4	165	10.3	13.2	16.2	19.1	22.0
Sugrue et al. [4]	76.5	-76.5	0.0	0.0	0.0	0.0	0.0

Table 5b. Prediction accuracy of existing nucleation frequency correlations

Nucleation frequency correlations	All data (%)		Percentile of data in given error bands (%)				
	MAD	MRD	± 10%	± 20%	± 30%	± 40%	± 50%
Cole [35]	61.2	-61.2	1.5	3.0	5.9	11.8	25.0
Zuber [36]	65.4	-65.3	1.5	4.4	8.8	11.8	20.5
Chu et al. [9]	98.2	-98.2	0.0	0.0	0.0	0.0	0.0
Ivey [38]	69.7	-69.7	0.0	0.0	1.5	3.0	8.8
Hatton and Hall [37]	77.4	-77.4	1.5	1.5	4.4	5.9	11.8
Situ et al. [40]	72.5	-72.5	0.0	1.5	1.5	3.0	5.9
Euh et al. [41]	86.8	86.8	0.0	0.0	4.4	5.9	23.5

Journal Pre-proofs

Table 6a. Prediction accuracy of the correlation proposed for departure diameter (Eq. (17))

Data	All data (%)		Percentile of data in given error bands (%)				
	MAD	MRD	± 10%	± 20%	± 30%	± 40%	± 50%
Present data (S2-wall slope of 37.5°)	16.3	0.14	27.3	69.7	87.9	100	100
Present data (S1-wall slope of 62.5°)	14.7	4.3	28.5	74.2	97.1	100	100
Holagh et al. [18] (S_1^U-wall slope of 0°)	16.7	-1.9	36.0	68.0	88.0	96.0	96.0
Holagh et al. [18] (S_2^U-wall slope of 45°)	18.0	-12.4	16.0	76.0	88.0	92.0	100
Holagh et al. [18] (S_3^U-wall slope of 90°)	24.3	-23.7	20.0	28.0	60.0	96.0	96.0
Average	18.0	-6.7	25.5	63.2	84.2	96.8	98.4

Table 6b. Prediction accuracy of the correlation proposed for nucleation frequency (Eq. (18))

Data	All data (%)		Percentile of data in given error bands (%)				
	MAD	MRD	± 10%	± 20%	± 30%	± 40%	± 50%
Present data (S2-wall slope of 37.5°)	22.7	3.0	39.4	60.6	69.7	84.8	87.9
Present data (S1-wall slope of 62.5°)	8.4	-2.1	65.7	94.3	100	100	100
Holagh et al. [18] (S_1^U-wall slope of 0°)	16.6	-3.2	44.0	72.0	84.0	88.0	96.0
Holagh et al. [18] (S_2^U-wall slope of 45°)	21.0	-20.0	28.0	52.0	68.0	88.0	100
Holagh et al. [18] (S_3^U-wall slope of 90°)	24.2	-24.2	28.0	40.0	56.0	76.0	96.0
Average	18.5	-9.3	41.0	63.8	75.5	87.4	96.0

Journal Pre-proofs

Journal Pre-proofs

Declaration of interests

☒ The authors declare that they have no known competing financial interests or personal relationships that could have appeared to influence the work reported in this paper.

☐The authors declare the following financial interests/personal relationships which may be considered as potential competing interests:

Shahriyar Ghazanfari Holagh: Project administration; Conceptualization; Data curation; Formal analysis; Investigation; Methodology; Visualization; Writing – original draft; Software; Validation

Mohammad Ali Abdous: Project administration; Conceptualization; Data curation; Formal analysis; Investigation; Methodology; Software; Writing – review & editing; Software; Validation

Prosun Roy: Formal analysis; Methodology; Software; Visualization; Writing – review & editing; Validation

Masood Shamsaiee: Data curation; Formal analysis; Investigation; Methodology; Visualization; Writing – original draft; Software; Validation;

Mahmood Shafiee: review & editing; Formal analysis

Hamid Saffari: Supervision; Resources

Luis Valiño: review & editing

Ronnie Andersson: review & editing

Journal Pre-proofs

1- Bubbles departure characteristics are studied in a U-shaped channel
2- High-speed photography is used as the measurement method
3- The effect of flow conditions on bubbles departure characteristics is investigated
4- A new correlation is proposed to predict bubbles departure diameter
5- A new correlation is proposed to predict bubbles nucleation frequency

Journal Pre-proofs